Effect of Directed Port Air Flow on Liquid Fuel Transport in a Port Fuel Injected Spark Ignition Engine

by

Robert J. Scaringe

B.S. Mechanical Engineering
Rensselaer Polytechnic Institute, 2005

SUBMITTED TO THE DEPARTMENT OF MECHANICAL ENGINEERING IN PARTIAL FULFILLMENT OF THE REQUIREMENTS FOR THE DEGREE OF

MASTER OF SCIENCE IN MECHANICAL ENGINEERING
AT THE
MASSACHUSETTS INSTITUTE OF TECHNOLOGY

JUNE 2007

Signature of Author:_____
Department of Mechanical Engineering
May 9, 2007

Certified by:_____
Wai K. Cheng
Professor of Mechanical Engineering
Thesis Supervisor

Accepted by:_____
Lallit Anand
Chairman, Departmental Graduate Committee

(this page was left intentionally blank)

Effect of Directed Port Air Flow on Liquid Fuel Transport in a Port Fuel Injected Spark Ignition Engine

by

Robert J. Scaringe

Submitted to the Department of Mechanical Engineering
on March 5, 2007 in Partial Fulfillment of the
Requirements for the Degree of Master of Science in
Mechanical Engineering

Abstract

With highly efficient modern catalysts, startup HC emissions have become a significant portion of the trip total. Liquid fuel is a major source of HC emissions during the cold start and fast idle period. Thus the control of liquid fuel, particularly during startup, is required for future engine designs. The effect of a turbulence plate, or charge motion control valve, on the port liquid fuel mass is examined.

A purging process was used to examine the effect of a charge motion control plate on the port fuel film mass. It was found that the charge motion plate can provide substantial reductions in both the total and downstream intake fuel film mass. These reductions are the result of the increased intake turbulence that results from the charge motion plate. This increased turbulence provides enhanced fuel – air mixing and increases port film strip atomization due to the increased viscous shear.

The effect of different film locations was postulated and backed experimentally. The downstream and valve films have the most immediate effect on the fuel delivery. Large upstream films, which can take thousands of cycles to develop, influence the fuel delivery on a much longer time scale.

In-cylinder hydrocarbon measurements were made. Despite the high level of scatter in the measurements, similar transient responses were observed for both CMCV open and closed. This similarity despite different film masses was attributed to different τ and χ values.

Thesis Supervisor: Wai K. Cheng
Title: Professor of Mechanical Engineering

(this page was left intentionally blank)

Acknowledgements

This research was generously supported by the Engine and Fuels Research Consortium at MIT. This consortium includes DailmerChrysler, Ford Motor Company, General Motors, and Saudi Aramco. In addition to their financial support, these companies provided technical guidance throughout this project.

I would like to thank Professor Wai K. Cheng for his support throughout this project. He was always available to help with all aspects of the project. I greatly appreciate his willingness to help solve any problems encountered. His immense technical knowledge, patience, and eagerness to assist make him a great advisor. I look forward to working with him on my PhD.

I also want to thank all those who have been there for me during my time at MIT. I am extremely grateful to have the support of my family. My dad is always there for me and is always a rock for me to lean on; his support is unparalleled. Additionally I want to thank all my friends for their love and support.

(this page was left intentionally blank)

Table of Contents

List of Figures

List of Tables

(this page was left intentionally blank)

Nomenclature

ASTM	American Society for Testing and Measuring
ABC	After Bottom Center
ATC	After Top Center
BBC	Before Bottom Center
CA	Crank Angle
COV	Coefficient of Variation of NIMEP
CP	Constant Pressure
CVI	Closed Valve Injection
ECT	Engine Coolant Temperature
EVC	Exhaust Valve Closing
EVO	Exhaust Valve Opening
FFID	Fast Flame Ionization Detector
FID	Flame Ionization Detector
HC	Hydrocarbon
ID	Inner Diameter
IVC	Intake Valve Closing
IVO	Intake Valve Opening
MAP	Manifold Absolute Pressure
MON	Motor octane number
NIMEP	Net Indicated Mean Effective Pressure
NVH	Noise, Vibration, and Harshness
OVI	Open Valve Injection
PFI	Port Fuel Injection
PW	Pulse Width
RON	Research Octane Number
RVP	Reid Vapor Pressure
SOI	Start Of Injection
UEGO	Universal Exhaust Gas Oxygen sensor
UTG	Unleaded Test Gasoline

CA50	Crank Angle location of 50% mass fraction burned
CA90	Crank Angle location of 90% mass fraction burned
mf_{film}	Mass of fuel in film
$mf_{in\text{-}cylinder}$	Mass of fuel in the in-cylinder charge
$mf_{injected}$	Mass of fuel injected per cycle
m_i	Mass of i
MW_i	Molecular Weight of i
n_i	Moles of i
τ	Tau from the from the τ-χ model
χ	Chi from the from the τ-χ model
x	Mole fraction
x_{res}	Molar residual fraction

(this page was left intentionally blank)

1 Motivation

The conversion efficiency of a fully warmed modern three way catalyst is in the upper ninety percents. However a typical catalyst does not become effective until it reaches a threshold temperature of approximately 300°C[a]. During a cold start the catalyst is significantly below its light-off temperature resulting in the release of a large portion of the trip total emissions (in particular hydrocarbon emissions). To reduce emissions during the startup, most vehicles now feature a small catalyst placed very close to the exhaust manifold in addition to a larger downstream catalyst. The close coupled catalyst warms up more quickly than the downstream catalyst helping to reduce cold start emissions.

As a result of the unfavorable thermal environment in the combustion chamber (and intake port for a PFI engine), a significant amount of fuel enrichment is required to provide enough vaporized gasoline for a robust engine start. This, in part, results in a large amount of liquid fuel entering the combustion chamber. Much of the liquid fuel which enters the chamber escapes the combustion process and subsequently evaporates during the exhaust process thus providing high cold start hydrocarbon emissions. Hydrocarbon emissions are closely regulated making a reduction in cold-start hydrocarbon emissions a top priority for future engine designs.

The reduction of catalyst light off time is an active area of research. The use of electric resistance [1], various catalyst shapes [2], gas burners [3], and secondary air injection [4] are several methods being examined to improve catalyst light-off time. Additionally various engine control strategies are being examined and used to provide faster catalyst light-off. Strategies such as retarded spark timing are being used in many engine designs to provide the catalyst with high enthalpy flow thus aiding catalyst light-off.

Another area of active research involves the reduction of engine out hydrocarbon emissions. Use of different injection timing, cam phasing, spark timing, and intake flow (through the use of a flow directing plate) during startup are being examined. Of course, the effect of these different strategies on exhaust enthalpy flow and thus catalyst light-off time are of important consideration.

---

[a] This is known as the catalyst light-off temperature.

As stated, a major source of cold-start HC emissions is liquid fuel entering the combustion chamber. A large percentage of this in-cylinder liquid fuel is sourced from fuel films in the intake port.[a] This liquid fuel is a large portion of the liquid fuel which enters the chamber does not vaporize before the combustion event. During the exhaust stroke a portion of this liquid fuel evaporates thus leading to high hydrocarbon emissions. The work examines the ability of a charge motion control valve (CMCV) to reduce the port liquid fuel film mass thus providing reduced in-cylinder liquid fuel during the cold start.

[a] For closed valve injection, intake films are the major mechanism by which liquid fuel enters the engine. With open valve injection, direct passage of liquid fuel droplets is very important. However for both open and closed valve injection, films in the valve vicinity are of the most importance. This is discussed in detail in Section 2.

2 Research background

2.1 Port fuel injection cold start HC emissions

In a port fuel injected engine, only part of the fuel injected per cycle reaches the engine's combustion chamber during that cycle. Conventional PFI injectors produce fuel sprays with Sauter Mean Diameters on the order of 150 μm. The inertial forces on these droplets are much larger than the drag forces. As a result a substantial portion of the injected fuel lands on port and intake valve surfaces[a]. Fuel vapor is formed by a combination of direct evaporation of the droplets, evaporation of the port wall film, evaporation of the fuel droplets strip-atomized from the wall film, and evaporation of liquid fuel within the combustion chamber from the cylinder and piston surfaces [5].

A significant source of hydrocarbon emissions during engine cold-start is the presence of liquid fuel within the combustion chamber. During the cold-start period the cylinder wall and piston top are relatively cool. A large portion of the liquid fuel which enters the chamber remains a liquid leading to the formation of in-cylinder films. These films escape the combustion event and the upward piston motion transfers much of the cylinder wall film to up nearer the exhaust valve where further fuel accumulation can occur. Vaporization of these film accumulations after the combustion event leads to substantial hydrocarbon emissions. Additionally in-cylinder fuel films on the cylinder wall and piston lands may flow into the crankcase leading to oil dilution problems [6].

While liquid fuel wall wetting on any surface in the combustion chamber will lead to increased HC emissions, it has been shown that the specific wetting location can have a substantial effect on the magnitude of the increase. Stanglmaier [7] used a spark-plug mounted directional injection probe to examine the effect of different fuel film locations within the combustion chamber. As one would expect, it was found that fuel films on the cylinder liner under the exhaust valves led to the largest increase in HC emissions. Fuel films on the piston top were found to give the second largest increase in HC emissions.

It is interesting to note the location of liquid fuel films within the combustion chamber during a cold start for a PFI engine. Using a gasoline-soluble dye and filter paper paced on the cylinder liner and piston surfaces, Kim [8] found that with open valve

[a] For direct vaporization of all of the injected fuel the fuel droplet diameter must be less than 10 μm [9].

injection (OVI) fuel films are predominantly formed on the exhaust side cylinder liner while with closed valve injection (CVI), fuel films are formed on the piston top and intake side cylinder liner. Witze and Green [10] applied imaging techniques to find similar results. Additionally it was found that fuel films formed on the underside of the intake valves and exhaust valves for CVI and OVI operation respectively.

The process by which liquid fuel enters the chamber differs for CVI and OVI. This accounts for the different in-cylinder film locations. Using a special transparent visualization engine, three major liquid fuel transport mechanisms have been identified [11]:

1. Forward flow strip atomization from the liquid fuel film on the valve seat and subsequent entrainment in the intake air flow
2. Fuel film flow
3. The squeezing of remaining liquid fuel on the valve seat during the valve closing

These mechanisms have been described and observed by many researchers [12-14]. When the intake valve opens at idling and part throttle conditions, the cylinder pressure is higher than the intake pressure resulting in backflow of burnt gases. This backflow of burnt gases strips fuel films on the valve and valve seat periphery. A portion of this stripped fuel is vaporized and the remaining fuel is carried upstream. Due to the downward motion of the piston the gas flow direction eventually reverses and the forward flowing intake gas then transports liquid fuel from the intake port and valve seat into the engine. The shear stress generated by the intake flow strips droplets from the liquid fuel film on the valve seat and valve head periphery and carries these droplets into the combustion chamber. This process is called forward flow strip atomization. Furthermore with the large intake fuel films associated with CVI, some fuel film may "dragged" by air-flow generated viscous shear directly into the combustion chamber, accumulating on the backside of the valve and cylinder head [9]. This dragging of the film is known as film flow. Film flow primarily occurs mid stroke when the intake port air velocity is highest [15]. When the intake valve closes, liquid fuel which remains on the valve head seal and valve seat is squeezed, in rather large droplets, back into the intake port as well as the combustion chamber.

It is very important to realize that the intake port fuel film mass/thickness is much greater for CVI[a]. Thus while forward flow strip atomization and valve seat film squeezing occur for both OVI and CVI, the amount of liquid fuel on the valve seat during both the forward flow and valve closing events is less for OVI. With OVI, a substantial amount of liquid fuel enters the cylinder by direct passage of airborne droplets past the intake valve.

Using a Phase Doppler Particle Analyzer (PDPA) in a special transparent visualization engine, Meyer [15] was able to measure the local size and velocity of liquid fuel droplets entering the combustion chamber parallel to the cylinder axis. Figure 2.1, taken from [15], relates the cycle position of each measured droplet (at a fixed location within the combustion chamber) to the time after engine start-up. While there is no information on droplet size or velocity, this plot illustrates the differences in the liquid fuel transport mechanisms between OVI and CVI and also shows how the mechanisms change as the engine warms up.

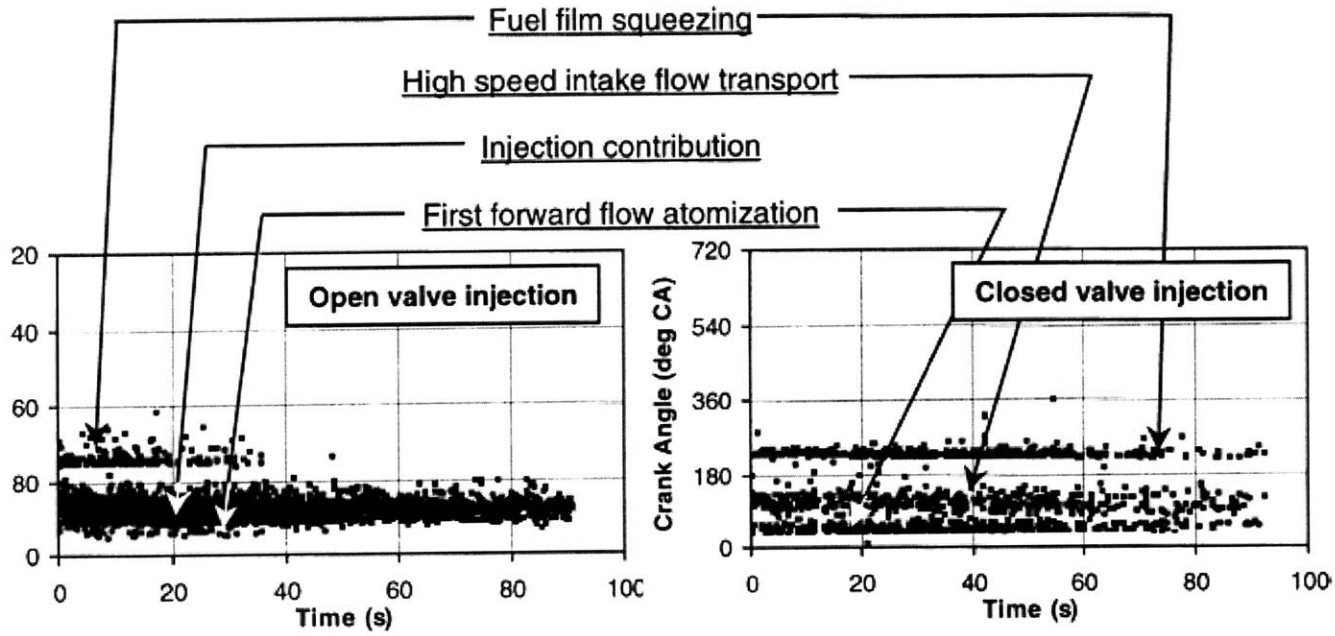

Figure 2.1: Differences in liquid fuel transport mechanisms between OVI and CVI [15]

[a] There are many fuel film locations within the intake port and manifold. Thus there is not a single film thickness. The film thickness on the valve head and valve seat periphery is of high importance; the film mass scales with the film thickness at these locations [16].

Note that although forward flow strip atomization occurs for both OVI and CVI, this mechanism is more significant for CVI operation as result of the larger fuel film in the intake valve vicinity. With OVI, the injection contribution is very strong and persists even after 90 seconds of engine operation. Fuel film squeezing from the closing intake valve is very distinct for both OVI and CVI; however this mechanism remains longer with CVI due to the larger fuel film present in the intake port.

2.2 Fuel film locations

The intake fuel film can be thought to occupy three conceptual film locations. A valve film, a downstream port film very close to the valve (and downstream the injector), and an upstream port film located far upstream of the valve. It is important to realize that an actual engine does not actually have three well defined films. Rather liquid fuel wets the walls in a more or less continuous manner. However the conditions and composition of the liquid fuel at different locations differ substantially resulting in vastly different residence times [9].

Upon injection the light ends of the fuel preferentially vaporize leading to film compositions that contain higher fractions of the heavier ends than the injected fuel[a] [13]. However the fraction of heavy ends varies considerably between the different film locations. The heavy end fraction in upstream films is higher than the downstream or valve films. This is largely the result of exhaust backflow. Under throttled operation, when the intake valve opens, the intake pressure is much lower than that of the cylinder. A strong backflow of exhaust gases results. This high velocity backflow shatters portions of the fuel film on the intake valve and valve seat periphery into very small droplets which are carried to upstream locations. The lighter ends of this shattered fuel readily vaporize leaving the heavier ends to be carried to upstream locations. Thus the upstream films contain higher fraction of the remaining heavier ends [17].

The surface temperatures at the upstream film locations are lower than the downstream film locations and much lower than the valve surfaces. This lower surface temperature results in reduced direct evaporation of surface fuel films.

[a] Note that as the wall temperature increases, the proportion of heavy ends in the film increases [13].

Upstream films often form in recessed areas where air flow is reduced, such as the injector recess. In this engine the closed CMCV plate provides a large area where airflow is reduced and accumulations can occur[a]. Films in these areas of limited flow experience substantially less strip atomization.

Furthermore the long path to the intake valve generally prevents any direct film flow from upstream locations [9]. Thus the fuel in the upstream films must first flow into the downstream films before it is eventually dragged, by viscous shear, into the combustion chamber.

Summarizing, fuel in the upstream films has a substantially longer residence time that in the downstream or valve films because [9]:

a. the composition will have a higher fraction of heavy ends
b. the temperature is lower,
c. the airflow may be reduced, and
d. the long path to the valve limits direct film flow.

In some cases fuel films or oil-fuel films/puddles can form at extreme upstream locations. These films do not actively participate in the fuel delivery process. As discussed earlier, the reverse backflow which occurs with throttled operation can transport fuel to upstream locations. Depending on the port/manifold geometry and the strength of the backflow fuel can be carried to extreme upstream locations. Additionally, under highly throttled conditions, very small amounts of lubricating oil can be carried upstream. In engines where the intake manifold runners have a bend or "U-shape" fuel and oil can accumulate and form sizable films or puddles. The temperature in these upstream locations is usually too low for any considerable vaporization to occur. Thus the size of these films is controlled only by the viscous shearing from the intake air. The engine used in this study featured U-shaped runners which resulted in the formation of these large puddles. Figure 2.2 provides a photograph of such an accumulation in the manifold runner after only 1000 fired cycles operated with a MAP of 0.43 bar.

[a] These accumulations can make engine calibration for transient operation very difficult.

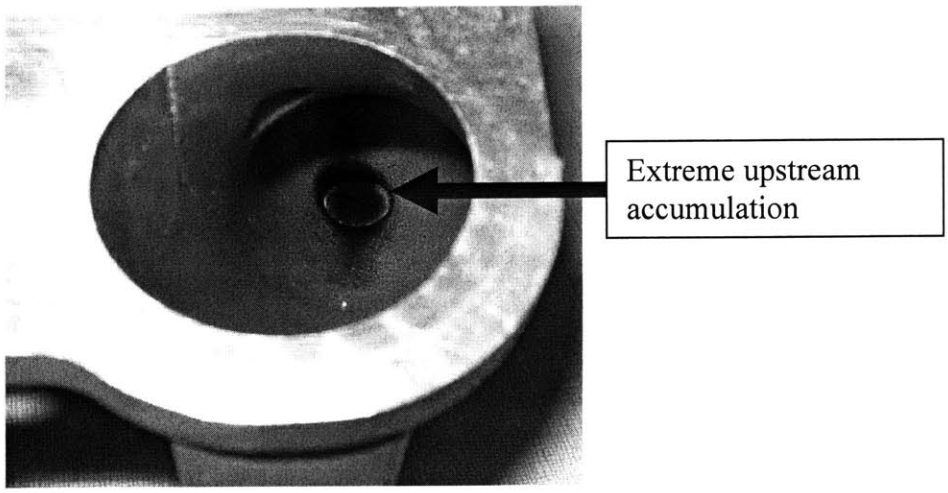

Figure 2.2: Fuel-oil accumulation in intake manifold U-shaped trap[a]

It is interesting to note that the use of the charge motion control valve (CMCV) dramatically reduced the formation of these large manifold runner accumulations. It is thought that the CMCV plate simply blocks the flow of oil and fuel from entering the manifold runner thus preventing this large accumulation.

It is important to realize that in an actual engine, the intake port surface temperature would increase to a maximum value of approximately 90°C[b]. As the coolant temperature increases the film mass is reduced dramatically [18].[c] However the films or puddles contained very far upstream, such as in the U-portion of a runner, do not see this temperature increase. It is also important to realize that high speed, open-throttle operation can substantially reduce the size of these films due to the increased viscous shear.

2.3 Objectives

A reduction in the downstream port and valve film mass will lead to a reduction in the amount of liquid fuel which enters the combustion chamber through the above discussed mechanisms. This reduction in the mass of liquid fuel entering the combustion chamber will provide for reduced cold start and fast idle engine out hydrocarbon emissions.

---

[a] The round ring seen in the photograph is a casting mark.
[b] The intake port surface temperature is essentially equivalent to the coolant temperature [13].
[c] At 90°C the fuel film has been shown to contain only the heavy ends of the fuel as the lighter more volatile ends have vaporized [13].

Previous work by Lee [19] found that a CMCV can substantially reduce cold start hydrocarbon emissions. This improvement is due to a reduction in the mass of liquid gasoline which enters the chamber. Using a gasoline-soluble dye and filter paper placed on the cylinder liner and piston surfaces Kim [20] showed qualitatively that a charge motion control plate can provide substantial reductions in cylinder liner and piston top fuel wetting.

The CMCV increases the intake air turbulence thus providing improved fuel-air mixing and improved forward flow strip atomization. This improved mixing and increased strip atomization (and subsequent fuel vaporization) are thought to result in reduced intake film mass. As discussed earlier, a reduction in port film mass will provide reduced in-cylinder liquid films. . This work examines the effect of a flow directing plate, or charge motion control valve, on the total liquid fuel film mass within the engine. Using film development data, the effect of the CMCV on the valve films is also quantified. Additionally the effect of the charge motion control valve on fuel delivery is examined.

(this page was left intentionally blank)

3 Experimental Apparatus

3.1 Modified port fuel injected spark ignition engine

Testing was performed on a production 1.8 liter, 4 valve per cylinder, port fuel injected Nissan QG18DE engine. The combustion chamber was a shallow hemisphere design with a centrally located spark plug as shown in Figure 3.1. The engine was modified to operate on one cylinder (cylinder #4). The specifications for the engine are provided in Table 3.1.

Table 3.1: Nissan QG18DE engine specifications

Displacement (per cylinder) [cm^3]	442.3
Stroke [mm]	88
Bore [mm]	80
Compression ratio	9.5
Valve timing	IVO: 5° BTC; IVC: 51° ABC
	EVO: 26° BBC; EVC: 2° BTC

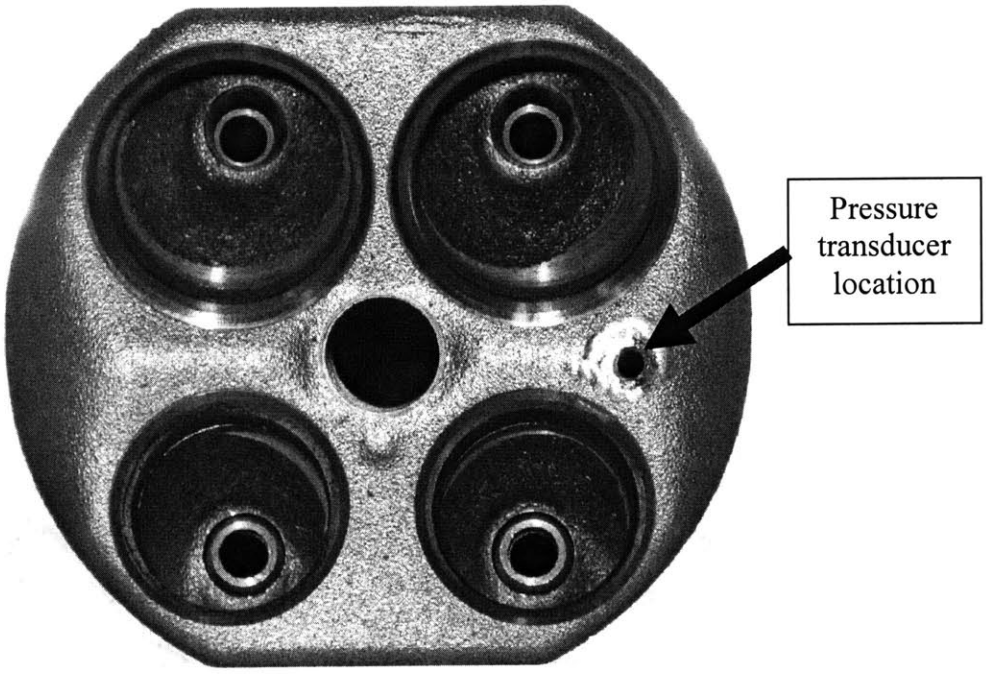

Figure 3.1: Photograph of Nissan head (chamber view)

3.1.1 Modified intake/exhaust system

The intake and exhaust manifold runners of cylinder #4 were separated from the remaining three runners. On the intake side, the three non-firing intake runners were open to the atmosphere and a block-off plate was installed between the upper and lower intake manifold halves. With the block-off plate installed, air-flowing through the plenum (and thus the air-flow meter located far upstream) could only enter cylinder #4. The intake manifold mounted on the engine is shown Figure 3.2. The stock throttle plate was removed and replaced with a large ball valve and fine needle valve connected in parallel. The ball valve provided coarse air-flow adjustment while the needle valve allowed for fine adjustment. A 55 gallon dampening tank was placed upstream of this throttle but downstream of the air mass-flow meter[a]. The air mass-flow was measured with a Kurz Instrument 505-9A-02 flow meter. The manifold absolute pressure (MAP) was measured using Data Instruments pressure transducer mounted in the intake plenum.

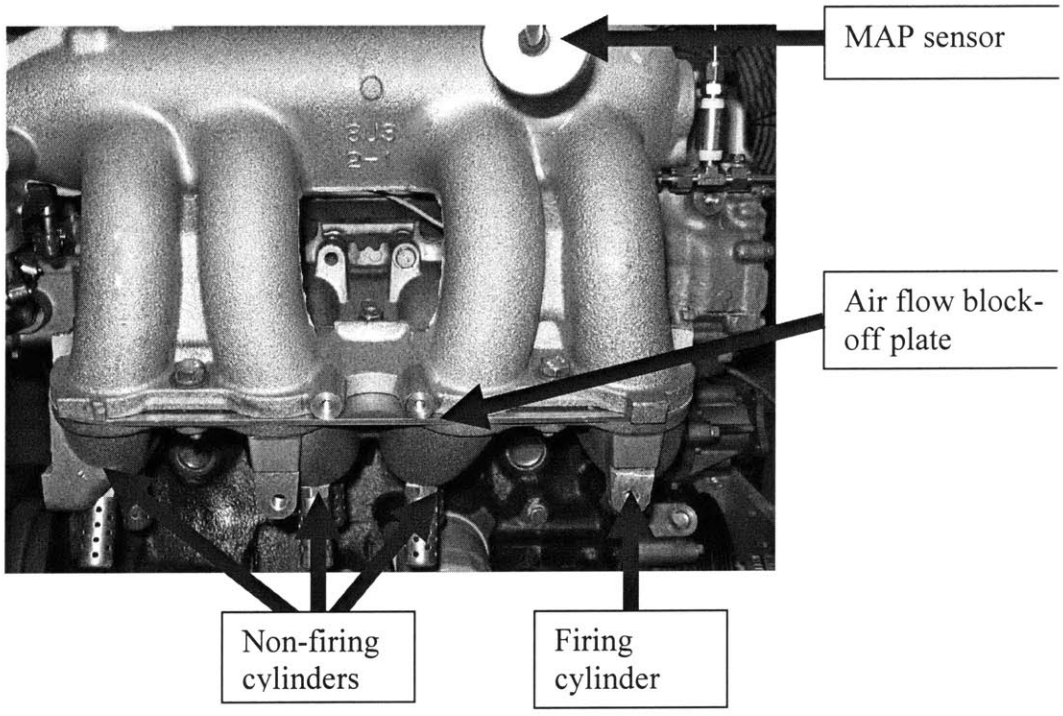

Figure 3.2: Intake manifold/plenum

[a] The dampening tank allowed for the steady flow to be accurately measured, dampening out the unsteady flow of air into the reciprocating engine. However accurate cycle-by-cycle air flow measurements were not possible with this arrangement.

3.1.2 Cooling system

The stock Nissan cooling system was removed. An external positive displacement pump, with a throttling bypass loop, was used to circulate coolant in a closed loop through the engine. The coolant loop also included a tube and shell heat exchanger which rejected heat to the city water supply. Depending on the desired coolant temperature, the flow of city water through this heat exchanger could be controlled. Upon exiting the heat exchanger, the coolant flowed into a large reservoir tank. This reservoir tank provided an increased volume of coolant allowing the coolant temperature to be more easily controlled. Additionally a VWR 1179PD, 1hp chiller was connected to the reservoir tank allowing the reservoir coolant temperature to be maintained at desired levels. The coolant temperature was measured with type-K thermocouples placed in the reservoir tank and at the inlet and outlet of the engine.

Unlike the stock cooling system, the coolant temperature was held constant for the tests performed. An actual engine employs a thermally controlled valve called a thermostat which prevents coolant flow to the radiator until the coolant temperature reaches roughly 85°C.[a] This allows the engine to warm up more quickly thus reducing hydrocarbon emissions and engine wear.[b]

The port fuel film mass is strongly affected by the metal surface temperature which in turn depends almost entirely on the coolant temperature and flow rate. Thus the absolute film mass and the film mass development depend highly on the coolant temperature and flow rate. In this study, we are not closely examining the film mass development nor are we concerned with the absolute film mass, rather the focus is the relative effect of a CMCV on the fuel film mass. Thus using a fixed coolant temperature, while not representative of an actual engine, is adequate for these experiments.

3.1.3 Fuel system

The stock fuel injector was used with the stock manifold mounting location, thus providing a fuel spray directed at the back of the intake valves. However the fuel rail was

[a] The two common thermostat ratings are 85°C and 91°C [21]
[b] The wear in a cold engine is higher as the oil is more viscous and its ability to coat the surface lubricating surfaces is reduced.

modified to allow flow through operation. This modification allowed the fuel to flow through the rail at a sufficient flow rate to allow the fuel temperature to be easily controlled. With the stock closed end configuration, the very slow fuel flow rate allows for substantial heat transfer between the fuel and the surroundings making precise temperature control of the fuel very difficult. A flat plate heat exchanger located downstream of the fuel pump was used with a controlled flow of city water to maintain the desired fuel temperature.

Commercial gasolines contain a very large number of different chemical species each with a different boiling point. Thus gasolines do not have a single boiling point but rather a range of boiling points. Fuel suppliers generally use the ASTM D86-05 distillation test and ASTM D323-06 Reid Vapor Pressure (RVP) test to quantify fuel volatility. The ASTM D86-05 [22] procedure measures the total volume percentage of a given fuel which evaporates at a given temperature. The temperatures at which 10, 50, and 90% of the fuel is vaporized are usually specified. As defined by ASTM D323-06 [23], the RVP is a measure of the absolute vapor pressure exerted by the liquid fuel (in an air filled vessel) at 37.8°C (100°F)[a]. Higher RVP values indicate more volatile fuels. The RVP is unique in that the combined effect of the different chemical species is captured in a single parameter. Thus this measure does not differentiate between a fuel with a very narrow distillation range and one with a much wider distillation range provided the cumulative vapor pressures are the same.

Unleaded test gasoline (UTG) from Chevron Phillips was used in these tests. The properties of this fuel are provided in Table 3.2.

Table 3.2: UTG-91 fuel properties [24]

Reid Vapor Pressure	62.1 kPa
Distillation range at 760 mmHG	
Initial boiling point	31.1°C
10%	50.0°C
50%	100.0°C
90%	160.6°C
End point (100%)	203.9°C
Research Octane Number (RON)	90.8
Motor octane number (MON)	82.8

[a] The RVP differs from the true vapor pressure of the fuel. This is the result of a small amount of fuel vaporization along with the pressence of water vapor and air in the test vessel.

The fuel injector was calibrated by removing the fuel rail from the engine and mounting it on a calibration fixture using flexible fuel lines. Only one injector was calibrated and the remaining three rail injector locations were plugged for the calibration procedure. The calibration fixture allowed the injector outlet to be securely inserted in a small graduated cylinder which was placed in an ice-water bath.[a] Fuel chilled to 0°C was injected for a set number of injections at various injection pulse widths. The total volume of fuel injected was measured and used to calculate the volume of fuel per injection for each of the pulse width settings. The amount of fuel vaporization was minimized by placing the graduated cylinder in an ice bath and chilling the injected fuel to 0°C. The calibration procedure was performed at three different fuel rail pressures (note that the injector outlet was at atmospheric pressure). Figure 3.2 shows the injector calibration curves obtained along with the linear curve fit equations. Notice that the R^2 values were all very close to one.[b]

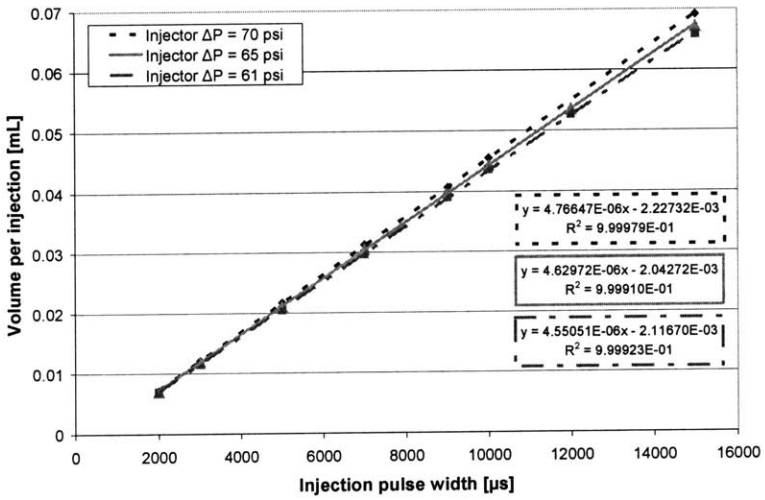

Figure 3.3: Injector calibration

3.1.4 Propane fuel system

Operation on propane facilitated several useful measurements. A separate intake manifold was modified to allow operation on propane. Propane was injected 3 mm upstream of one of the intake valves using a copper tube with a 1.5 mm ID. A small

[a] While the injector fit snuggly into the graduated cylinder it was not an air tight seal which would have resulted in a decreasing pressure difference across the injector as the graduated cylinder was filled with fuel.

[b] Note that the volume of fuel delivered is proportional to $(\Delta P)^{0.5}$.

needle valve was used to throttle the flow of propane from a pressure regulated tank into the intake port. Additionally a toggle valve was placed immediately before the intake manifold entrance allowing the propane flow to be quickly shut off. The use of small diameter copper tubing and the placement of the toggle valve as close as possible to the manifold entrance helped to minimize the amount of propane that was contained within the injection tube. At the engine speed and load used in these tests (1400 RPM, 1.43 bar NIMEP), the amount of propane contained in the short length of tubing from the toggle valve to the tube end was roughly 20% of a stoichiometric mass of fuel. This was important for cut fueling tests, in which the propane supply was abruptly cut off.

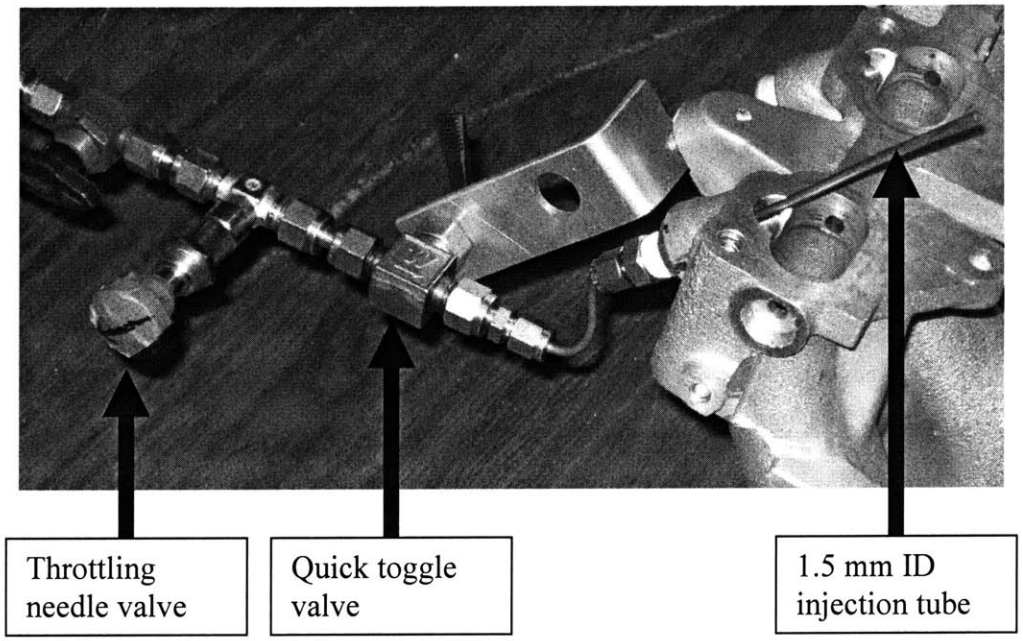

Figure 3.4: Propane injection device

3.1.5 Engine controller

The spark and fuel injection timing were controlled using a MIT designed controller. The controller used a Kontron adio1600 board for basic operation.
A fixed startup routine was developed for all tests. This 14 cycle start-up routine was designed to provide a robust startup while quickly dropping the injected fueling PW to the steady state amount. It was important not to use lambda feedback as this would have allowed unequal amounts of fuel to be injected. Figure 3.1 provides the fueling pulse width for the 14 cycle start-up routine.

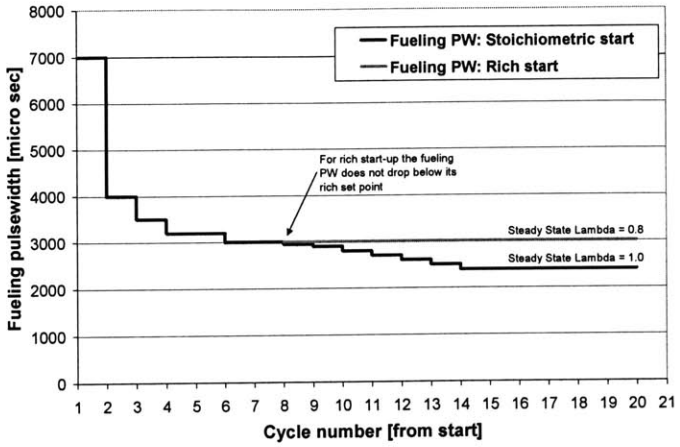

Figure 3.5: 14 cycle engine start-up routine

3.1.6 Engine encoder

A crankshaft mounted digital encoder was used to obtain precise piston crank angle (CA) location. A digital pulse was produced every CA along with an additional pulse at bottom center (BC) of every rotation. These signals were used to trigger the data acquisition system and with the engine controller for control of the spark and fuel injection timing.

3.1.7 Charge motion control valve

The stock Nissan charge motion control plate was used. The plate was located between the intake runner and intake port. This plate was the combined swirl/tumble or "swumble" type and had a 25% open flow area. A fixture was constructed to hold the plate either open or closed ensuring that the open and closed positions were the exact same for all tests. A photograph of CMCV plate installed in the intake manifold along with the positioning fixture is shown in Figure 3.6.

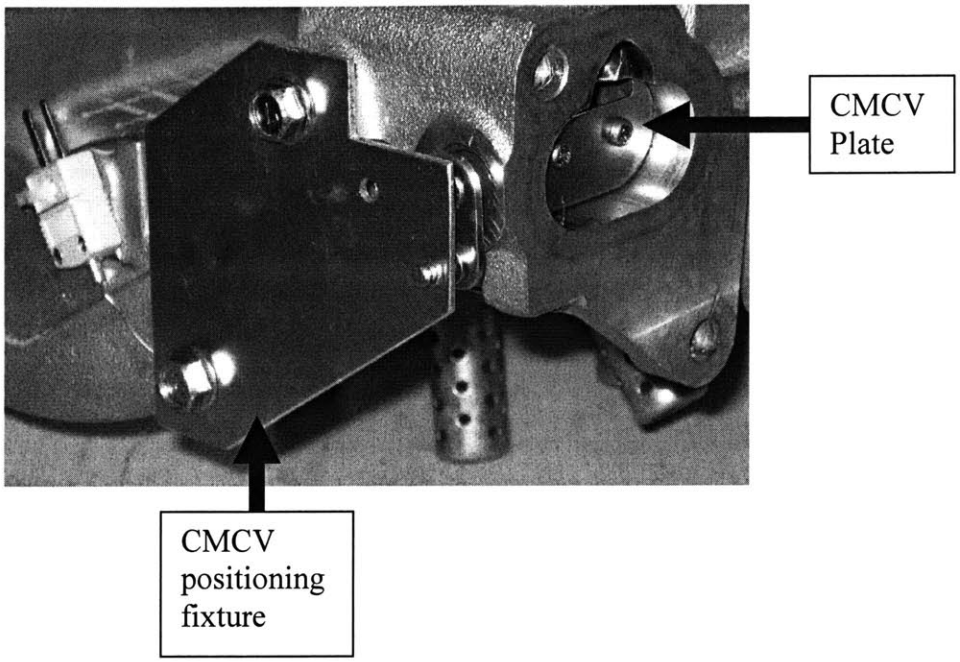

Figure 3.6: CMCV installed in intake manifold

3.2 Data acquisition

A National Instruments PCI-6025E multi-function I/O board and BNC 2090 connector board were used with Labview to acquire data. The Labview data acquisition program was triggered with the crank angle pulse from the shaft mounted digital encoder and data was recorded every crank angle. In-cylinder pressure, MAP, air mass flow, and the hydrocarbon measurement signal were recorded. Additionally, thermocouple readings from the intake manifold, exhaust manifold, coolant inlet/outlet, and fuel rail were recorded by hand.

3.2.1 In-cylinder pressure measurements

The in-cylinder pressure is very important for determination of the net indicated mean effective pressure (NIMEP), coefficient of variation of NIMEP (COV), and burn duration. A Kistler 6051A piezoelectric pressure transducer was mounted in the cylinder head, 32 mm off center, as shown previously in Figure 3.2. The measured pressure acts on a diaphragm which compresses the quartz with a force proportional to the pressure. Under loading the quartz yields an electrostatic charge. A high impedance cable transfers this charge to a charge amplifier which converts the charge signal to a voltage signal. A Kistler 5010 dual mode amplifier was used to amplify the charge signal.

The piezoelectric signal was proportional to the rate of pressure change therefore a reference pressure was needed to determine the absolute in-cylinder pressure. The standard practice is to reference the pressure on an individual cycle basis to the 20 CA average centered on BC of the intake event [25]. At BC of the intake stroke the piston is stationary and the intake valves are still open, thus the in-cylinder pressure at moderate engine speed is essentially equal to the MAP. In this work the MAP was recorded every crank angle. The pressure was pegged using the MAP average from 10 CAD before BC to 10 CAD after BC compression.

3.2.2 Fast Flame Ionization Detector (FFID)

A Cambustion HFR400 FFID was used for all hydrocarbon measurements. This device consists of hydrocarbon sampling head and gas handling/electronics subsystem. The gas handling system provided precise control of the gas and vacuum requirements.

Figure 3.7 provides a schematic of the sampling head. The sampling head differs from a conventional FID in that the sample gas is mixed with the fuel gas at the fuel nozzle exit. This provides a much faster response as the sample is drawn directly into the flame chamber. As in a conventional FID, the hydrocarbon concentration of the sample stream is determined by measuring the number of ions generated when the sample is introduced to a non-HC flame (hydrogen was used in these tests). The number of ions produced is proportional to the number of carbon atoms burnt in hydrocarbon form[a] [26].

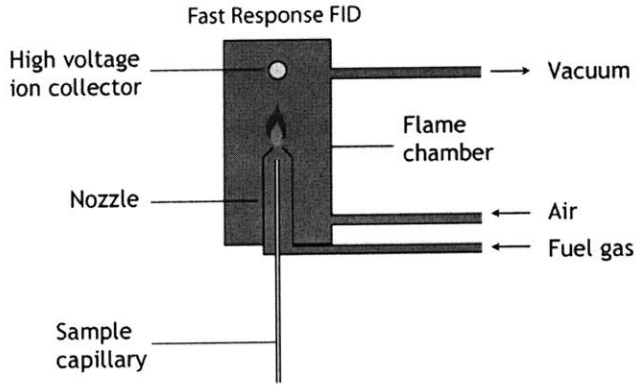

Figure 3.7: Cambustion FFID sampling head schematic [27]

[a] The FFID signal drifts over time and thus needs to be calibrated regularly.

A constant pressure (CP) chamber was fitted to the sampling head for the measurements in this work. The CP chamber removes the effect of pressure fluctuations on the sample flow rate into the flame chamber. In this configuration, the sample flows from the source to the CP chamber through a heated sample line.[a] The pressure of the CP chamber is set low enough to ensure that the sample is drawn from the source under all conditions.[b] Both the flame chamber and CP chamber have bleed flow regulators to help maintain constant pressure within them. However these bleed flow regulators maintain constant pressure over a relatively long time scale; the rapid pressure fluctuations are dampened by the large (relative to sample flow fluctuations) CP volume. With a large enough CP volume, the sample flow fluctuations do not affect the pressure difference across the sample capillary thus providing a constant sample flow rate into the flame chamber. It is very important to realize that the sample capillary draws the sample from the incoming sample flow and not the CP volume. The CP volume acts only as a damper and does not provide the sample flow. Figure 3.8, taken from [26], provides a diagram of the CP chamber and its associated plumbing. The heated sample line attaches to a device labeled tee-top. The inner diameter of the tee-top is larger than that of the heated sample line which ensures that sample velocities within the tee-top are reduced from the sample line values. The FID tube (or sample capillary) forms a tee with tee-top allowing a static tapping of the fluctuating sample flow. The CP chamber simply acts to dampen any pressure fluctuations in the sample flow and does not provide sample to the FFID chamber.

[a] The sample line is heated to prevent any water or fuel from condensing out of the sample flow.
[b] A typical value for the CP chamber vacuum is 350 mmHG vacuum. A typical pressure drop across the sampling capillary is 100 mmHG [26].

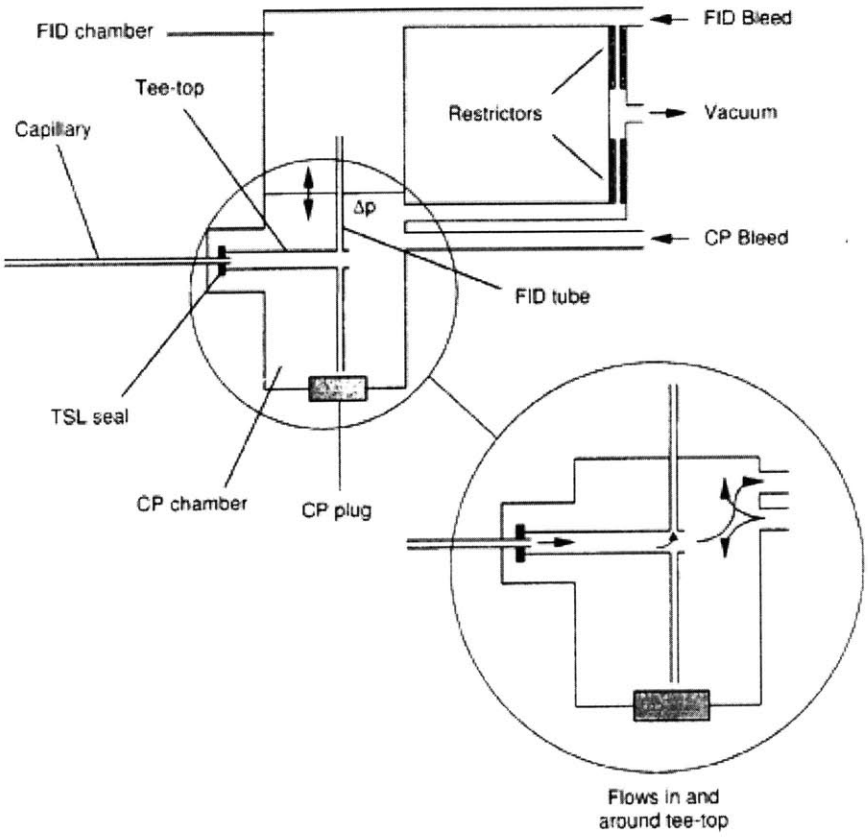

Figure 3.8: Diagram of FFID CP chamber [26]

Thus the response is not affected by fitting a very large CP volume. For the in-cylinder tests performed a sampling head with a 2500 cc CP chamber attached was used ensuring that the large sample pressure fluctuations were adequately damped. For the measurements from the exhaust port a 5 cc CP chamber was used.

For the in-cylinder tests the FFID was calibrated before and after each test using a mixture of propane and air with a HC concentration comparable to the high in-cylinder values seen. A volume flow rate controller was used to mix the propane and air. For the manifold HC measurements the FFID was calibrated before every other test using a bottled mixture of propane and nitrogen with a propane concentration of 1500 PPM.

A Kistler sampling spark plug was used to measure the in-cylinder HC concentration. The sampling spark plug, shown in Figure 3.9, features an offset electrode allowing for a small sampling probe to be threaded into the plug body.

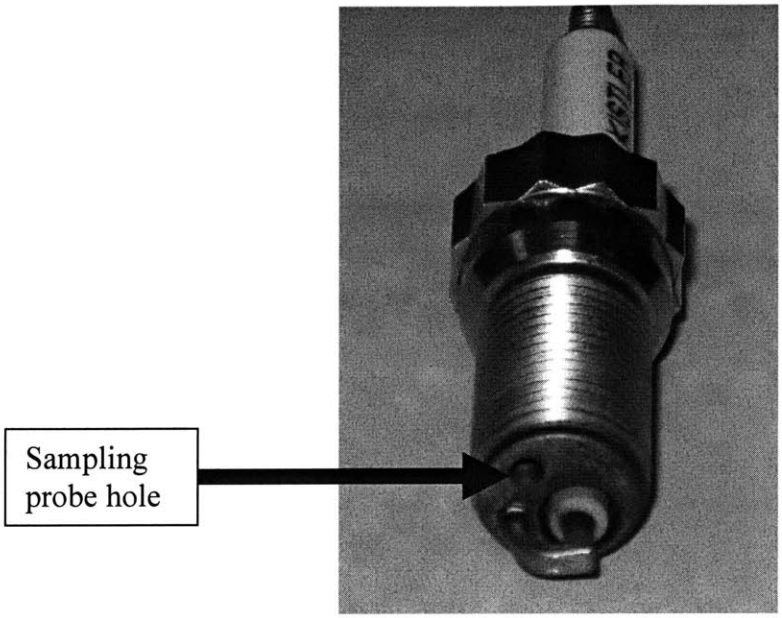

Figure 3.9: Kistler sampling spark plug

4 CMCV Background

The burning velocity during the rapid-burning phase[a] of the combustion process scales approximately with the charge turbulence intensity [28]. Thus for a fixed engine load, increasing the turbulence intensity results in a faster combustion process. An engine with faster combustion is less sensitive to cyclic variations in mixture composition, temperature, and pressure thus providing improved engine stability [28].

Throttling in a SI engine substantially reduces the intake charge density. Additionally, throttling increases the burned gas fraction which slows down both flame development and propagation resulting in a longer combustion process. This slower combustion process results in lower engine stability. Increasing the charge turbulence intensity at low load/speed can provide much improved engine stability.

A charge motion control valve is a device which is used to increase the intake turbulence intensity. A CMCV device features a rotating turbulence plate, similar to a butterfly throttle plate but with a portion removed, placed at the entrance of the intake port. The CMCV is closed to enhance combustion stability during low load/speed operation but is opened for high load/speed conditions.

The effect of the charge motion plate on the burn rate for this test engine operating at 1400 RPM, with stoichiometric fueling and a fixed throttle setting providing a MAP of 0.43 bar is shown in Figure 4.1[b].

---

[a] The rapid-burning phase of the combustion process is the interval of the burning process during which the bulk of the charge is combusted. It is defined as the interval between the end of the flame-development stage (usually taken to be a mass fraction burned of 10%) and the end of the flame propagation process (usually taken to be a mass fraction burned of 90%)

[b] The burn rate profile was computed using the in-cylinder pressure measurements. A single-zone model utilizing an energy release approach (First law of Thermodynamics) described in [29] was used with measured pressure data to compute the burn rate profile.

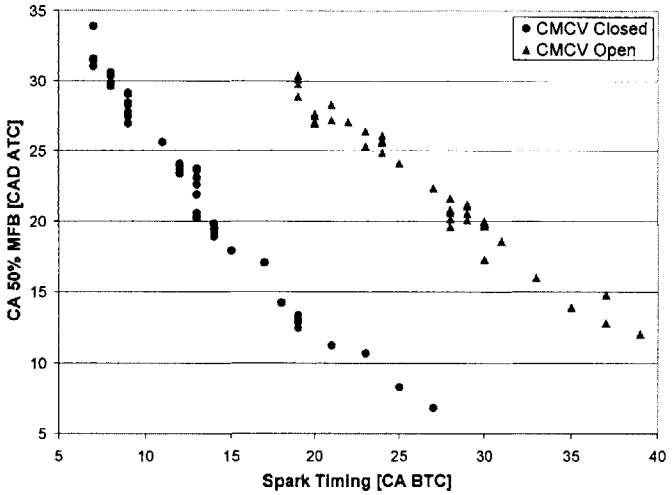

Figure 4.1: Effect of CMCV on the 50% MFB location

At these operating conditions, for a given spark timing, use of the charge motion plate advances the location of the CA50 by more than 10 CA. For fixed throttle setting and fueling, the NIMEP scales with the CA50. Figure 4.2 provides the NIMEP as a function of the CA50 for the data points in Figure 4.1.

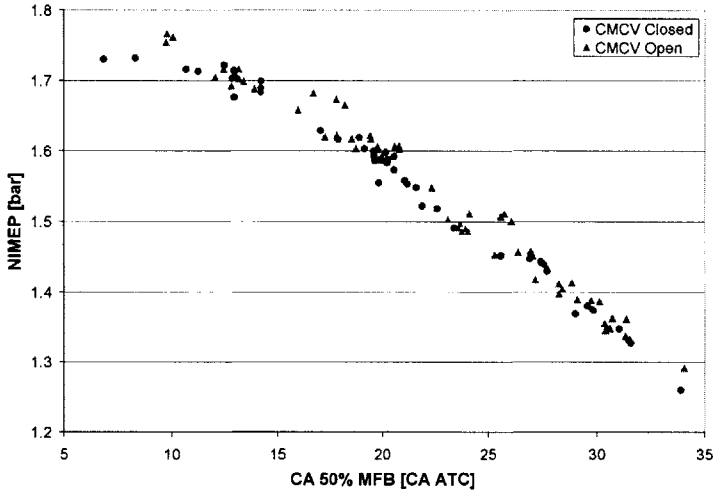

Figure 4.2: NIMEP vs. CA50

The average exhaust temperature, measured at the exit of the exhaust port, scaled slightly better with the CA90 than with the CA50 as is seen by comparing Figures 4.3 and 4.4.

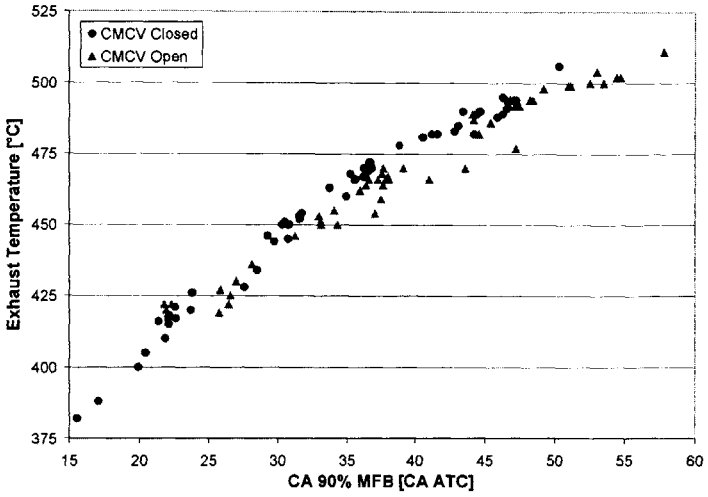

Figure 4.3: Exhaust temperature vs. CA90

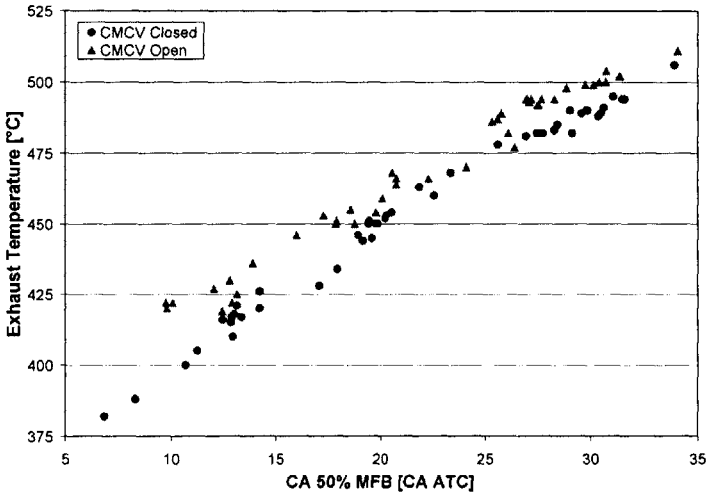

Figure 4.4: Exhaust temperature vs. CA50

A CMCV significantly improves the burn rate at part load conditions which provides improved engine stability for a given CA50 as shown in Figure 4.5. However as shown in Figure 4.6, this reduction in COV is smaller for a given average exhaust temperature.

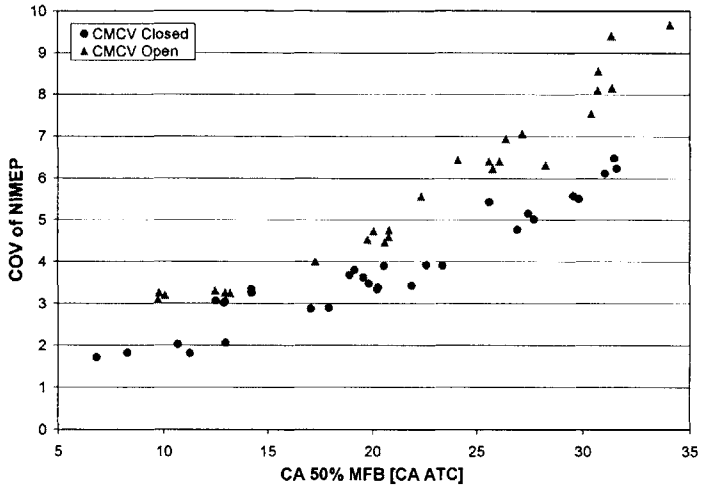

Figure 4.5: COV vs. CA50

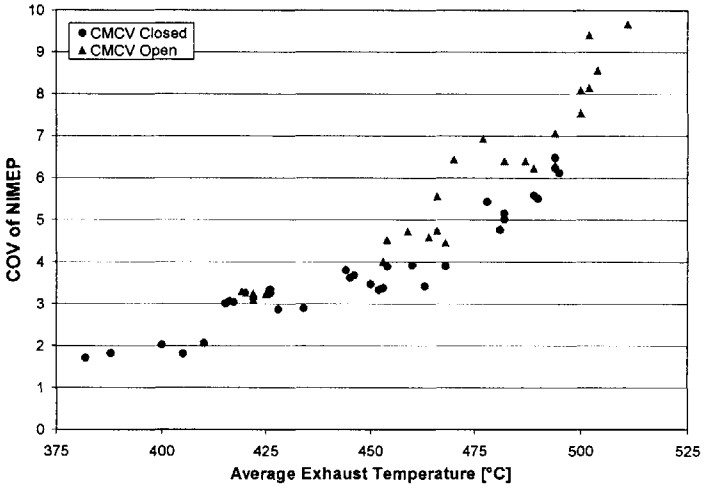

Figure 4.6: COV vs. average exhaust temperature

Thus, while a CMCV can be used to allow heavy spark retard during the engine warm-up period, the effect of retarding the spark timing on the exhaust enthalpy flow is largely offset by the faster burn rate.

A CMCV device imparts increased turbulence to the intake air. In addition to providing faster combustion, this increased turbulence is thought to improve the air-fuel mixing. The higher velocity of the directed flow increases viscous shearing of the fuel films. This allows increased forward flow strip atomization of the fuel films.

While the CMCV does have advantages it is not without drawbacks. Cost is a major issue; the use of a CMCV can increase the cost of an engine by 2-5% [30].

Additionally use of a CMCV complicates the engine calibration. This is the result of liquid fuel which can build up on the downstream side of the charge motion plate. When the CMCV opens, this liquid fuel, which was previously not active in the fuel delivery, is either entrained in the inlet flow or is pulled (by viscous shear) into the downstream port film. Additionally fuel can be strip atomized from films on the CMCV plate as it opens. It is difficult to adequately account for these fuel contributions and a rich spike in fueling is often the result.

It is important to note that CMCV devices have also found application in direct injected engines. While the effect on the port film mass and intake port mixing is no longer relevant, the increased swirl and tumble of the intake air has been shown to enhance in-cylinder fuel vaporization and fuel-air mixing resulting in better cold-start behavior [31].

(this page was left intentionally blank)

5 Fuel film experiments

5.1 Liquid fuel film measuring procedure

The liquid fuel film mass was estimated by firing a motored engine for a specified number of cycles and then disabling the fuel injection and ignition.[a] After cutting the fuel, the engine was motored to purge all the liquid fuel films from the engine. Throughout the entire experiment the rotational speed of the engine was held constant at 1400 RPM. A Cambustion HFR400 Fast FID sampling probe placed in the exhaust port, approximately 8 cm from the exhaust valve, was used to measure the exhaust HC concentration with resolution of ~0.1 ms. The measured HC concentration at the time of the fueling/ignition disable is shown in Figure 5.1.

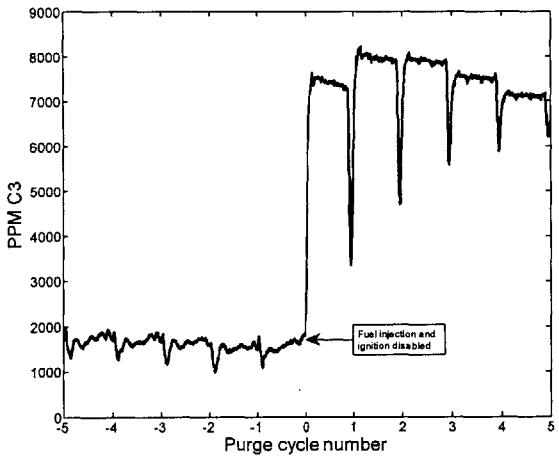

Figure 5.1: Exhaust HC concentration vs. number of purge cycles during fueling cut

For each purge cycle, the measured HC concentration has a flat plateau. This plateau corresponds to the exhaust port HC concentration during the valve closed period. With the exhaust valve closed the port flow is minimal and the measured HC concentration is representative of that purge cycle. The HC concentration of each purge cycle was determined using a 300 crank angle average of the plateau.

The sharp spikes between the purging plateaus are the result of exhaust backflow during the motored operation at the time of the exhaust valve opening. For these tests the

[a] The fuel injection was disabled after a complete injection. The spark was disabled after the combustion of this last fuel injection.

engine was operated throttled. Thus, for a non-firing cycle, at the time of the exhaust valve opening the in-cylinder pressure was lower than the exhaust port pressure resulting in a reverse blow-down. These spikes are an artifact of the FFID behavior during this reverse blow-down process and do not correspond to actual hydrocarbon levels[a].

The average purge cycle HC concentration was used with the measured air mass flow rate through the engine in the following equation to compute the total mass of hydrocarbons contained within that purge cycle.[b, c]

$$m_{fuel\ \ per\ \ purge\ \ cycle} = m_{air\ \ per\ \ purge\ \ cycle}\left(\frac{x_{HC1}}{1-x_{HC1}}\right)\left(\frac{MW_{HC1}}{MW_{air}}\right) \tag{5.1}$$

Figure 5.2 provides the measured hydrocarbon concentration for the first 30 purge cycles for both gasoline and propane operation.[d] The average hydrocarbon concentration values are also shown.

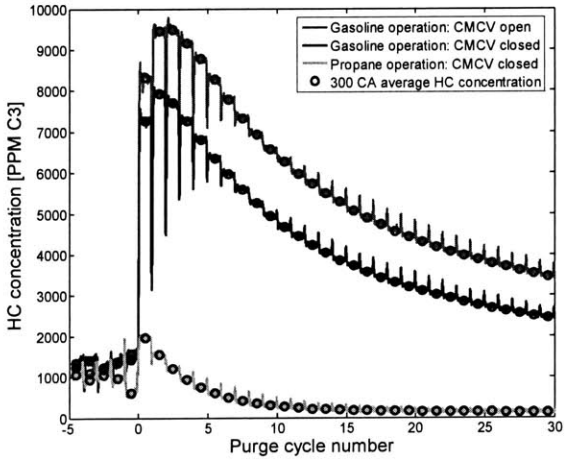

Figure 5.2: Gasoline and propane purging HC concentration

[a] This reverse blow-down results in the sucking back of CP chamber gas into the tee-top. The CP chamber is filled with a mixture of gas samples from previous cycles.

[b] The carbon to hydrogen ratio of all the emitted hydrocarbons is equivalent to that from the gasoline (UTG-91 in these experiments). This assumption is quite accurate because a large majority of the hydrocarbons emitted from the non-firing engine come from liquid gasoline films.

[c] Note in equation 5.1 that the average air mass flow rate was used to compute the mass of air in each purge cycle as the instantaneous air mass flow exiting the engine was not measured. A complete derivation of equation 5.1 can be found in Appendix A.

[d] For the gasoline data in Figure 5.2 the engine was fired for 250 cycles. For the propane data, the engine was fired for 30 seconds (350 cycles).

As seen qualitatively in Figure 5.2, the CMCV provides a substantial reduction in the purged hydrocarbon concentration. Note that the purged hydrocarbon concentration is significantly less for propane operation.

With propane operation there are no liquid fuel films in the intake port/manifold. The small jump in hydrocarbon concentration at the fueling cut was due to the unburned propane gas which remained in the intake and injection apparatus after the fueling was disabled. As discussed earlier, this propane system injects propane at a fixed rate into the intake port. At the time of the fueling cut, approximately 20% of a stoichiometric charge remains in the injection tube. Thus the decay seen in the propane curve is the result of this unburned propane charge combined with propane present in the port and residual exhaust gas from the last firing cycle. The decay takes several purge cycles as the propane diffuses from the injection apparatus and mixes with the intake air.

5.1.1 Non-film hydrocarbon contributions

Equation 5.1 calculates the total mass of hydrocarbons contained in each purge cycle. This mass contains hydrocarbons from sources other than intake port liquid fuel films. During the initial purging cycles, the mass of hydrocarbons in each purge cycle is sourced almost entirely from intake port fuel films. However after many purge cycles the mass of hydrocarbons in each purge cycle contains an increased fraction of non-film sources. This is because initially the very active downstream portion of the port fuel film is being purged thus providing very high exhaust hydrocarbon concentrations which dwarf any other contributions. The other purging hydrocarbon sources include the residual exhaust, evaporation of cylinder wall oil layers, evaporation of very thick films in the intake port (built up over time from the extremely heavy ends of the fuel), evaporation from extreme upstream films, and fuel desorption from the oil.

The effect of residual burnt gases is small. As can be seen in Figure 5.2, the firing exhaust hydrocarbon concentration is much lower than that of the first purge cycle. Furthermore, shown in Table 5.1, the residual fraction at these operating conditions is less than 20% for both the CMCV open and closed.[a] Thus within a few purge cycles the

[a] The residual gas fraction was measured in the engine for both the charge motion control valve open and closed and is discussed in later sections.

percentage of the exhaust gas which remains from the final firing cycle becomes insignificant.

Table 5.1: Remaining exhaust gas from final firing cycle

Purge cycle	CMCV Open	CMCV Closed
1st purge cycle	19.45%	17.16%
2nd purge cycle	3.78%	2.94%
3rd purge cycle	0.74%	0.51%
4th purge cycle	0.14%	0.09%
5th purge cycle	0.03%	0.01%

The magnitude of the combined fuel desorption and oil evaporation sourced hydrocarbon emissions were examined as described here. The engine was fired on gasoline for ten minutes with the load set to 1.5 bar NIMEP with the intent to preload the oil with gasoline. After ten minutes of continuous gasoline operation the engine was shut down without any film purging process.[a] At this point the intake manifold was removed and the intake port and manifold surfaces were thoroughly dried of any fuel films. The engine was then allowed to sit for an hour to ensure that any remaining liquid fuel within the engine had time to evaporate. After reassembling, the engine was motored, with the engine coolant temperature fixed at 26°C, and the resulting exhaust concentration was measured. The hydrocarbon concentration present in the exhaust was assumed to be the result of fuel desorbing from the liner oil layers and the slow evaporation of these oil layers. A plot showing this motoring exhaust concentration is provided in Figure 5.3. While not shown, a steady state concentration of roughly 57 PPM C_3 was reached after roughly 3500 purge cycles[b]. The decay seen in Figure 5.3 is thought to be the result of decreasing levels of fuel desorption.

[a] The engine can not be instantly stopped, thus there were several unavoidable purge cycles as the rotating engine was brought to a halt.

[b] Again note that the motored engine was heavily throttled resulting in substantial oil flow into the chamber.

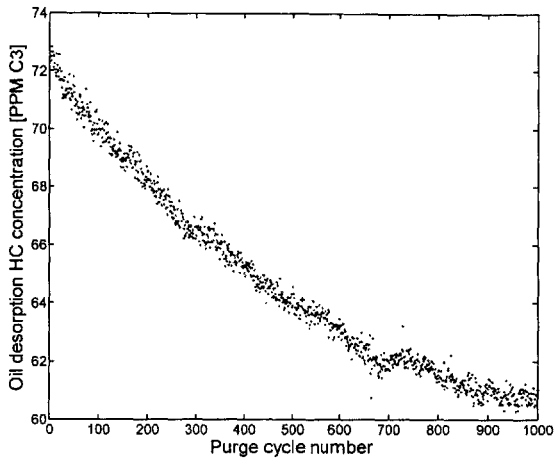

Figure 5.3: Oil desorption sourced hydrocarbon concentration vs. purge cycle (engine cool)

It is very important to note that these emissions correspond to a cool, non-firing engine. For the actual film purging process, during the initial purge cycles the liner is still hot from the combustion resulting in higher oil vaporization/fuel desorption emissions. To demonstrate this, the engine was operated on propane. After 5 minutes of stoichiometric propane operation with the MAP set to 0.43 bar, the fueling was disabled. The engine was then motored for several thousand cycles. After 18 purge cycles, the average exhaust port hydrocarbon concentration was 150 PPM C_3. The purged hydrocarbon concentration then slowly declined over approximately 3000 purge cycles to a steady state value around 57 PPM C_3. The higher initial hydrocarbon concentration is thought to be the result of increased oil layer vaporization, due to the higher liner temperature. To allow the fueling disable details to be clearly seen, the first 100 purge cycles are shown Figure 5.4. This test was repeated several times with equivalent results.

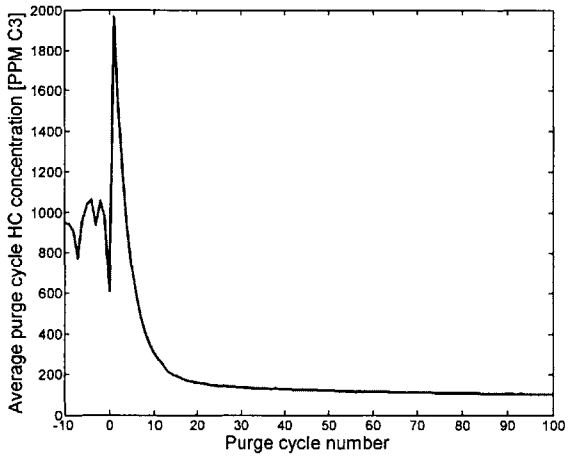

Figure 5.4: Average exhaust port HC concentration during propane stop fueling test

5.1.2 Estimating the port fuel film from purging HC measurements

In determining the total port film mass, the engine was not simply purged until the exhaust hydrocarbon concentration reached zero. Instead it was purged until the exhaust hydrocarbon concentration reached a carefully selected value. This steady state criterion was selected based on the non-firing information presented above.

In propane fueling/ignition disable tests, an average exhaust port hydrocarbon concentration of 150 PPM C_3 was reached after 18 purge cycles. After 100 purge cycles the exhaust hydrocarbon concentration was ~105 PPM C_3. These emissions are the result of oil vaporization. In a gasoline fired engine fuel desorption from the oil is also occurring.

A steady state criterion of 150 PPM C_3 was selected. In determining the total film mass, the engine was purged until this concentration was reached. The mass resulting from this contribution was then subtracted from the total mass.

The assumption that the hydrocarbon concentration due to non-film contributions (primarily oil vaporization/fuel desorption) is constant at 150 PPM C_3 simplified the calculations while providing a conservative estimate of the total film mass. Again the goal was to determine the effect of a CMCV on the intake port fuel film mass. This did not require that the absolute film mass be known with extreme accuracy. Furthermore hundreds of purge cycles are needed before this concentration reached. Stopping the

purging process at 150 PPM C_3 excludes the very inactive heavy ends present in upstream locations. As discussed previously, these heavy films can remain in the engine for very long periods of time.

The relative magnitude of the steady state criterion and purged exhaust HC concentration are shown in Figure 5.5.

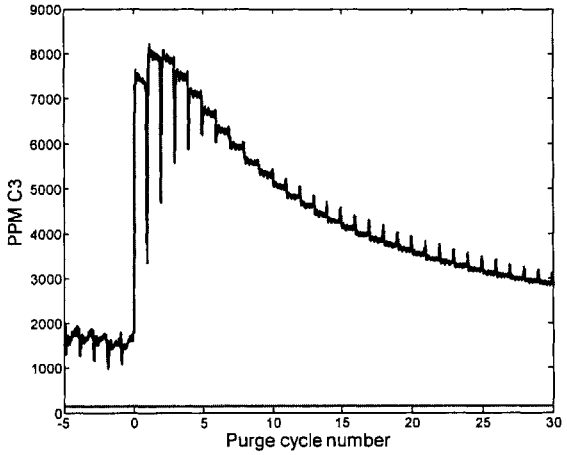

Figure 5.5: Comparison of exhaust HC concentration and steady state criterion

5.2 *Liquid fuel film results*

Unless specified otherwise all the results presented are for 250 fired cycles. The selection of 250 fired cycles was made as this provides sufficient time for a substantial film build-up without the formation of large upstream films. Additionally the fixed 14 cycle startup routine was used for all tests and the spark timing was set to provide equivalent CA50 for both CMCV settings. The operating conditions used for these fuel film tests are summarized in Table 5.2.

Table 5.2: Fuel delivery operating parameters

Engine speed	1400 RPM
MAP	0.43 bar
Ignition timing CMCV open	29 CA BTC
Ignition timing CMCV closed	14 CA BTC
Injection timing	450 CA ABC compression (CVI)
Fuel rail pressure	60 psig
Fuel temperature	23.5°C ± 0.5°C
Coolant temperature	26°C ±0.5°C
Ambient air temperature	31°C ±1.5°C
Steady state lambda	1.01 ±0.005

5.2.1 Effect of the CMCV setting

The effects of the CMCV on the film mass are presented qualitatively in this section; more detailed quantitative results are presented later.

The effect of the CMCV on the purged hydrocarbon concentration is clearly seen in Figure 5.6. Note that only the first 140 purge cycles are displayed and many more cycles are needed before the 150 PPM C_3 criterion is met. With the CMCV open, the purge cycle hydrocarbon concentration is higher throughout the entire purging process.

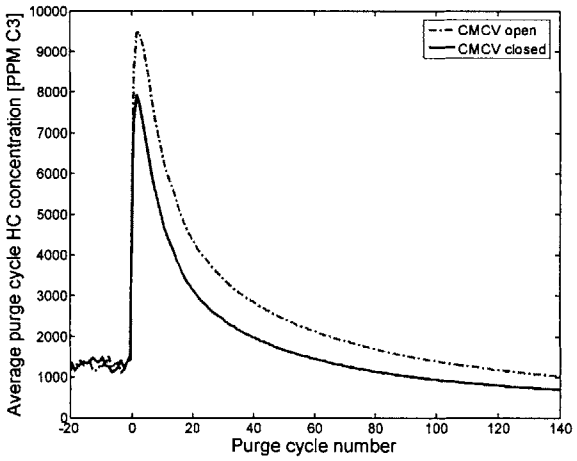

Figure 5.6: Average purge cycle HC concentration vs. purge cycle

Figure 5.7 shows the cumulative film mass as a function of the purge cycle for the entire purge process. The cumulative film mass refers to the sum of film mass computed for all purge cycles up to a given purge cycle. Thus the cumulative film mass at the fifth purge cycle is the sum of the film mass calculated for purge cycles one through five.

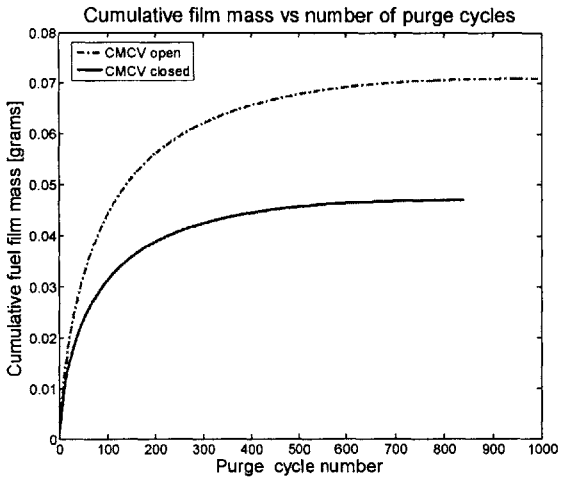

Figure 5.7: Cumulative fuel film mass vs. purge cycle: Entire purge process

Figure 5.8 provides a closer look at the cumulative purge mass for the first 30 purge cycles. As can be seen, the CMCV setting has an effect on the purged film mass from the first purge cycle.

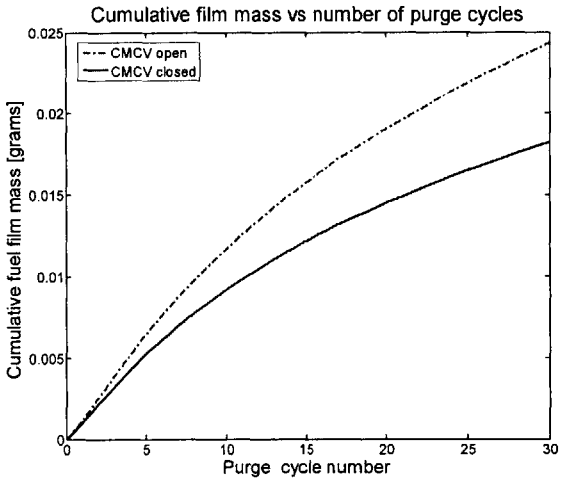

Figure 5.8: Cumulative fuel film mass vs. purge cycle: Initial purge process

5.2.2 Effect of the number of fired cycles

Figure 5.9 shows the measured total film mass as a function of the number of fired cycles for both CMCV open and closed at coolant temperatures of 26°C and 41°C. Note the large number of fired cycles that are required before the measured total film

mass reaches a steady value[a]. The engine lambda reaches a steady value far earlier as shown in Figure 5.10.

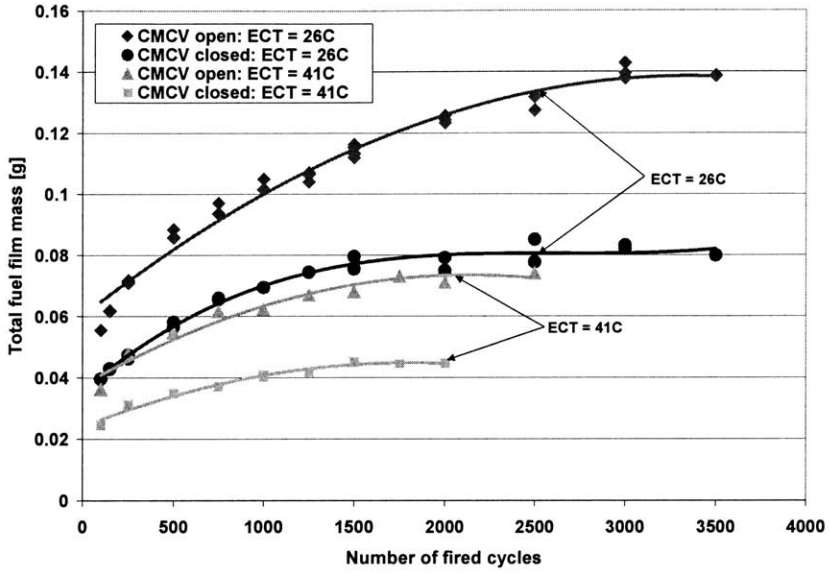

Figure 5.9: Total film mass vs. number of fired cycles

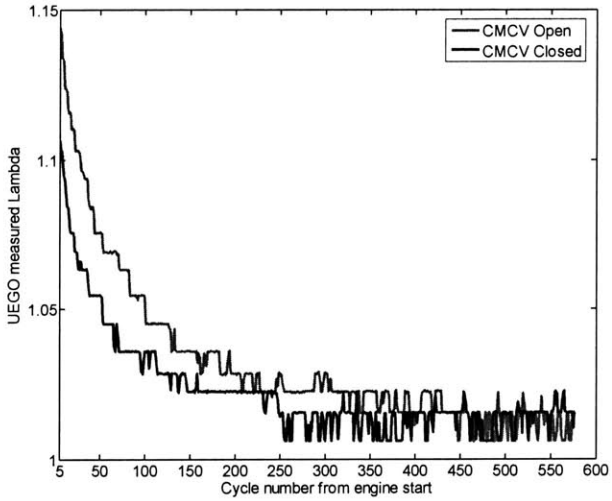

Figure 5.10: UEGO measured lambda vs. firing cycle (ECT = 26°C)[b]

[a] It is important to realize that Figure 5.9 is a plot of the total fuel film mass (calculated using the 150 PPM C3 criterion) as a function of the number of fired cycles. The similar appearance to the cumulative film mass plots (in which cumulative film mass is a function of the purge cycle number) can result in confusion.

[b] It is important to note that this transient response is slower than a production engine. In a production engine lambda feedback is used to more quickly provide stoichiometric fueling. Here a 14 cycle start-up routine was used after which the fueling pulse width was set to its steady state value.

There is a discrepancy in development time of the measured film mass and the in-cylinder fuel delivery measured with the lambda sensor; the fuel delivery reaches steady state much earlier than the total fuel film mass. This is a result of the different behavior of the upstream and downstream films. As discussed previously, much of the fuel in the upstream films does not enter the engine directly but is instead pulled into the downstream film and eventually dragged into the engine by the viscous shear from the flowing air. Upstream films can form in areas where the air-flow is significantly reduced such as in the injector recess. The film in these areas can slowly build-up until a steady state value, limited by air-flow, is reached. Once the steady state accumulation is reached, the flowing air will shear or strip fuel from these films as they attempt to grow larger.

It is the downstream and valve films that directly contribute to the fueling of the engine [9]. Thus the upstream film mass can slowly grow while the fuel delivery is essentially constant. For the upstream film to increase in mass, the amount of fuel which enters it must be greater than the amount that leaves. Obviously for the fuel delivery to be relatively constant, the upstream film mass must grow very slowly. That is, the fraction of each injection which contributes to the buildup of the upstream film must be very small. While this fraction is very small, the cumulative effect over many injections can be quite large.

Figures 5.11 and 5.12 show the effect of the number of fired cycles on the measured cumulative film mass with the ECT equal to 41°C for the entire and initial purge processes respectively. While the total film mass is different for 250 and 1000 fired cycles, the cumulative film mass during the first 20 purge cycles is essentially equivalent for a given CMCV setting.

This nearly identical behavior (for a given CMCV setting) during the first 20 purge cycles is thought to be the result of nearly identical downstream films. Thus while the total film mass is different, the downstream and valve film contribution to the fuel delivery are very similar and represent the predominate contribution to the fuel delivery. However, after these 20 purge cycles, the presence of the larger upstream films begins to take effect as the fuel from the upstream film is pulled into the downstream location and eventually into the engine.

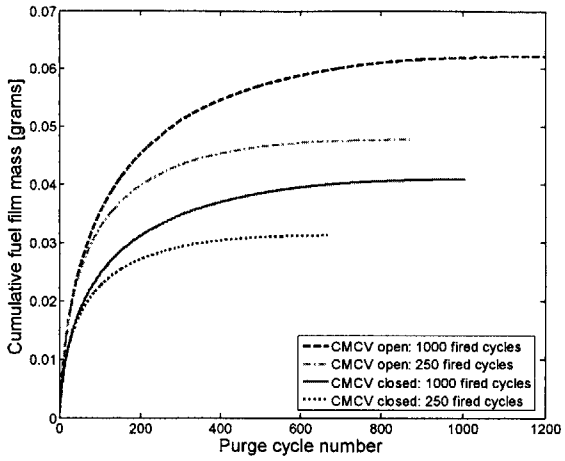

Figure 5.11: Cumulative film mass (ECT = 41°C): Entire purge process

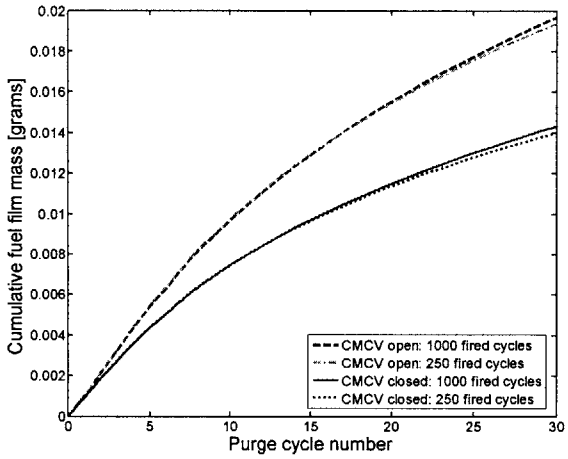

Figure 5.12: Cumulative film mass (ECT = 41°C): Initial purge process

This equivalence in the initial purge cycles can also be seen by observing Figure 5.13 which shows the average hydrocarbon concentration for the first 250 purge cycles.

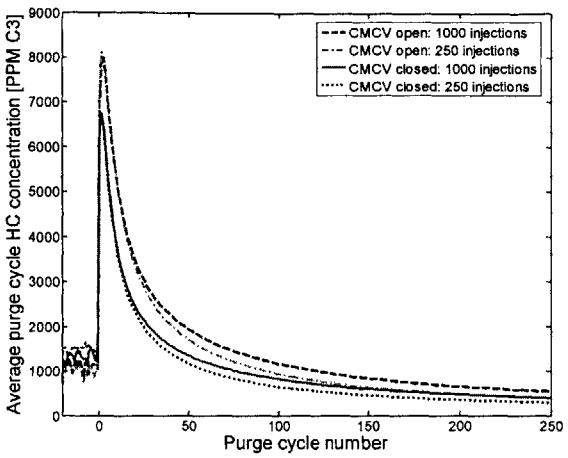

Figure 5.13: Average purge cycle HC concentration vs. purge cycle (ECT = 41°C)

Note from Figure 5.13 that the purged HC concentration with the CMCV open is initially higher than with the CMCV closed for both 250 and 1000 fired cycles. However after roughly 200 purge cycles the HC concentration for the CMCV open with 250 injections falls to that of the CMCV closed with 1000 injections. This is because initially the downstream and valve films dominate the purging process. However after 200 purge cycles purge cycles the contribution of the larger upstream film (due to the greater number of fired cycles) outweighs the downstream and valve films contribution.

The approximate contribution of each injection to the build-up of port films can be computed using the slope of the curves in Figure 5.9[a]. The slope of these curves at each injection represents the contribution of that injection to film build-up. Using the fitted curves shown in Figure 5.9, the percentage of each injection used to supply the buildup of the port film was computed and the results are plotted in Figure 5.14[b] .

[a] Figure 5.9 is a plot of total film mass as a function of the cycle number.
[b] Note in Figure 5.14 that the injection (fired cycle) number starts at 100.

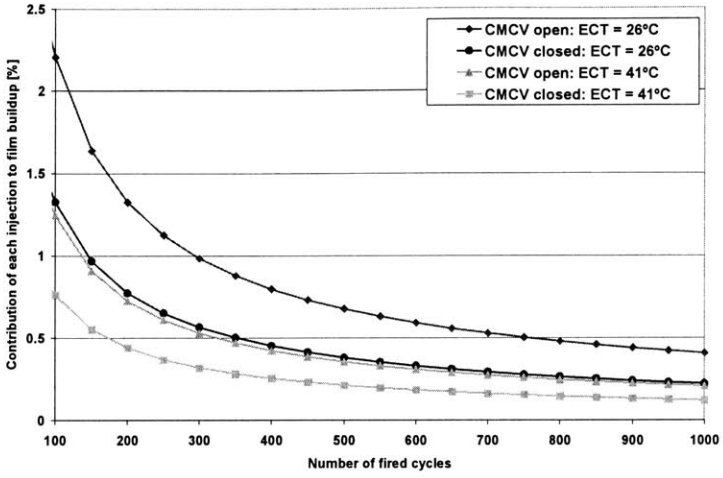

Figure 5.14: Contribution of each injection to film buildup

It is during the first 100 or so cycles that the substantial build-up of the downstream and valve films occurs. The fuel delivery approaches steady state as downstream and valve films fully develop and the fuel lost to film build-up becomes a very small percentage. It is this small non-zero percentage that leads to the slow build-up of the upstream films. Note the CMCV setting and coolant temperature have a sizable affect on the percentage of injected fuel which contributes to film build-up.

5.2.3 Effect of the engine coolant temperature

As seen in Figure 5.9 increasing coolant temperature provides reduced film mass. This is because the port film mass decreases with increasing port surface temperature. The port surface temperature is proportional to the coolant temperature, thus increasing coolant temperatures will result in reduced port film masses. This can also be seen in Figure 5.16 which provides the cumulative film mass as a function of the purge cycle for the entire purging process (data for 250 fired cycles). Figure 5.17 provides a closer view of the initial purge cycles; note that the effect of the coolant temperature on the cumulative film mass is observed from the very first purge cycle.

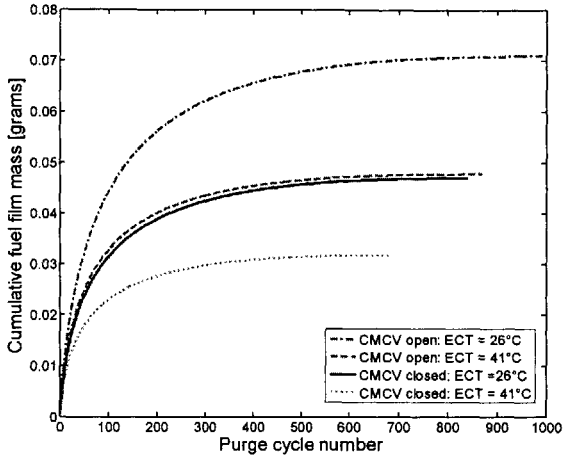

Figure 5.15: Effect of coolant temperature on cumulative film mass: Entire purge process

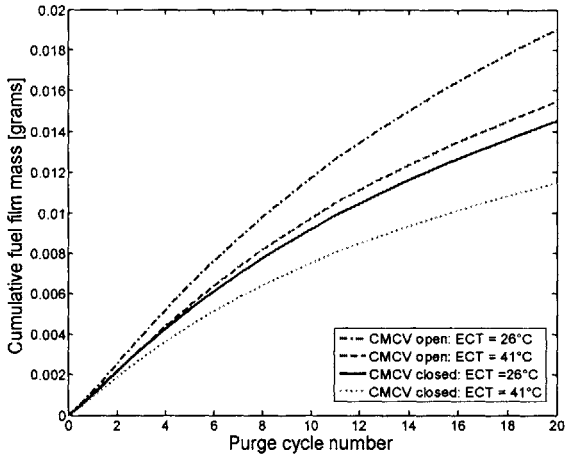

Figure 5.16: Effect of coolant temperature on cumulative film mass: Initial purge process

Figure 5.18 provides a plot of the ratio of the cumulative film mass for the CMCV open case to the CMCV closed case. This curve is almost identical for the two coolant temperatures demonstrating that the relative purging behavior, of the CMCV open to CMCV closed, is the very similar at the two coolant temperatures.

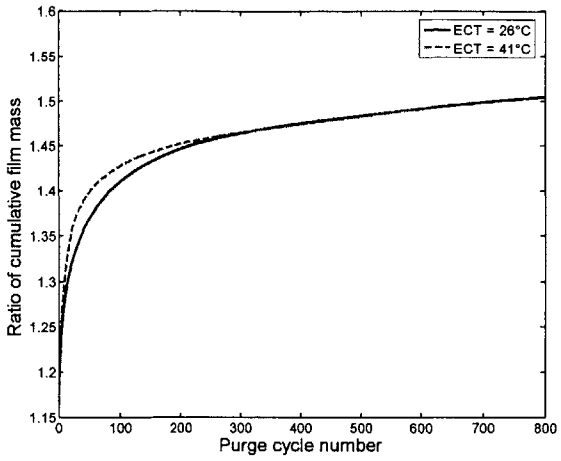

Figure 5.17: Ratio of CMCV open to CMCV closed cumulative film mass vs. purge cycle

Again it should be noted that in the tests performed, the coolant temperature was fixed. However, an actual automobile engine utilizes a thermostat, which prevents coolant flow to the radiator, until the coolant temperature reaches 85°C.

5.2.4 Effect of Injection timing

The effect of the fuel injection timing was examined. Figure 5.19 provides measured total film mass as a function of injection timing. Notice that the measured film masses (for closed valve injection) are greater than those found earlier. These tests were performed several months after the earlier tests and the fuel was not changed. While the fuel tank was properly sealed some of the lighter ends may have managed to escape leaving a less volatile gasoline mixture. Additionally the air temperature in these tests was 23°C whereas in the earlier tests was 34°C. It should be noted that previous studies have found that the intake air temperature has little effect on the vaporization of fuel droplets [32]. However the ambient air temperature greatly influences the manifold surface temperature. Thus while the values found in these tests may not be comparable to earlier values they show the effect of the injection timing.

Closed valve injection results in substantially larger port films. Note that with closed valve injection, the start of injection (SOI) timing did not have significant effect on liquid fuel film mass. With open valve injection, the film mass increases with later injection. This is because the later spray does not encounter the hot exhaust backflow.

This hot exhaust backflow assists fuel vaporization. Note that the engine does not run well at very late OVI as there is too little time for sufficient fuel vaporization. Thus testing could not be performed at late open valve injection timings.

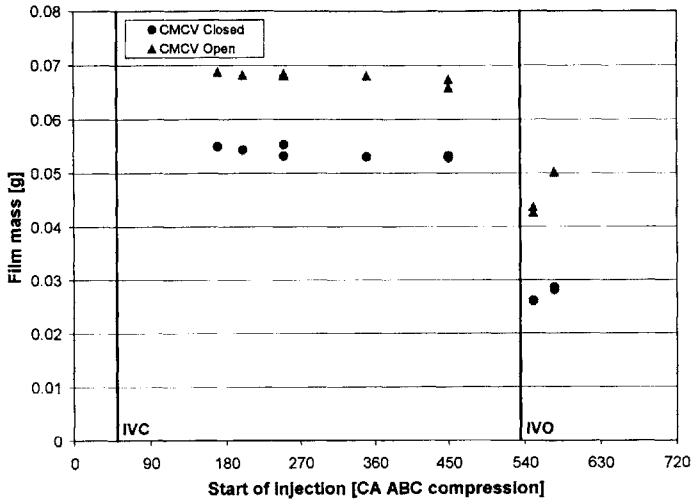

Figure 5.18: Total film mass vs. start of injection timing

6 Fuel delivery experiments

6.1 Measurement procedure

The transient response of the in-cylinder air-fuel ratio to a step change in the fueling was measured. The in-cylinder air-fuel ratio was determined from in-cylinder hydrocarbon concentration measurements. The response to both a rich step and lean step in fueling were examined.

A Kistler sampling spark plug was used with the FFID to measure the in-cylinder HC concentration. The pre-flame mixture hydrocarbon concentration can be determined from in-cylinder hydrocarbon measurements, such as that shown in Figure 6.1[a].

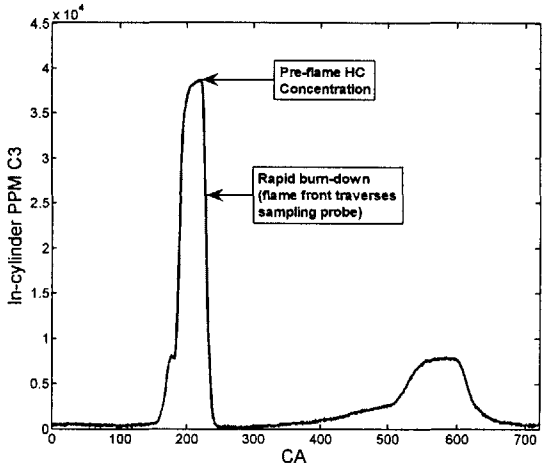

Figure 6.1: Typical in-cylinder HC trace from FFID

The relationship between the in-cylinder air-fuel ratio and the measured pre-flame hydrocarbon concentration is given below. The complete derivation for this equation is provided in Appendix B.

$$\left(\frac{m_{air}}{m_{fuel}}\right)_{in-cyl} = \left\{\left(\frac{1-x_{res}}{x_{HC1}}\right)\left(\frac{MW_{fuel}}{MW_{HC1}}\right)-1\right\}\frac{MW_{air}}{MW_{fuel}} \tag{6.2}$$

The calculation of the in-cylinder air-fuel ratio from the measured in-cylinder hydrocarbon concentration requires that the molar residual gas fraction (x_{res}) be known. Many models currently exist for predicting this, however these fuel delivery experiments

[a] Note that the FFID signal is plotted without correction for the sampling transit time, so the displayed CA does not correspond exactly to the actual CA values.

are performed at a single operating point allowing for direct measurement. Direct measurement also captured the effects of the charge motion control plate.

6.1.1 Measurement of the residual gas fraction

A successive dilution method was used to measure the residual gas fraction. This method is relatively simple and has been shown to provide very accurate results [33-35]. To eliminate any liquid fuel film effects the engine was operated on propane. After letting the engine reach steady state, the ignition is switched off while continuing the fueling. The residual gas in the chamber is successively diluted with fresh charge. After several motored cycles the in-cylinder HC concentration approaches that of the inlet mixture. Referring to Figure 6.2, the molar residual gas fraction is equal to the ratio A/B. In this work a 20 cycle average of A and B were used.

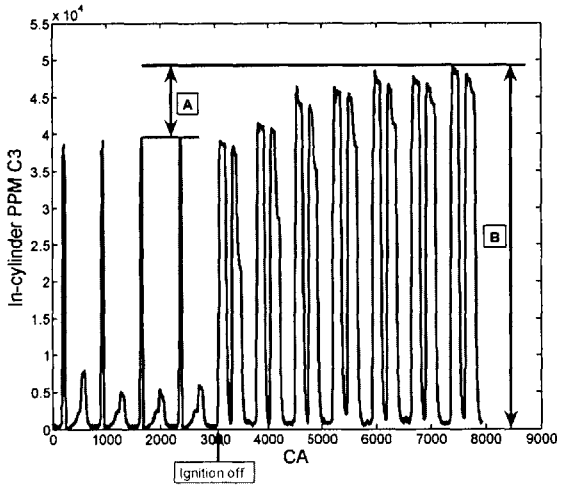

Figure 6.2: Residual gas fraction measurement

Table 6.1 provides the residual gas fraction values computed from in-cylinder hydrocarbon measurements. Six points were taken at three different ignition timings for both CMCV open and closed. For the range considered, the effect of the ignition timing was negligible.

Table 6.1: Measured residual gas fraction results

CMCV	Ignition timing [CA BTC]	Average residual gas fraction	Standard deviation
Open	20	19.45%	0.51%
Open	29	19.45%	0.55%
Open	37	19.93%	0.20%
Closed	9	17.16%	0.40%
Closed	14	17.16%	0.35%
Closed	19	17.74%	0.42%

6.2 Fuel delivery results

The fueling step was performed after 1000 fired cycles to achieve a relatively steady film buildup. The fixed 14 cycle startup routine was used for all tests. The spark timing was again set to provide equivalent 50% mass fraction burn location for both CMCV settings. However the spark timing was advanced relative to the film mass measurements providing slightly less noise on the in-cylinder FFID measurements. Closed valve injection was used for all the tests. The operating parameters for these fuel delivery tests are provided in Table 6.2.

Table 6.2: Fuel delivery operating parameters

Engine Speed	1400 RPM
MAP	0.43 bar
Ignition timing CMCV open	37 CA BTC
Ignition timing CMCV closed	19 CA BTC
Injection timing	450 CA ATC compression (CVI)
Injections before fueling step	1000
Rich fueling step	$\lambda = 1.01$ to $\lambda = 0.8$
Lean fueling step	$\lambda = 0.8$ to $\lambda = 1.08$

The in-cylinder measurements had significant scatter however they still provide some valuable information about the fuel delivery process. The observed transient responses for both CMCV settings were very similar.[a] It is important to realize that the film mass alone does not determine the transient response of the fuel delivery. The τ-χ model provides an approximate equation of for fuel delivery and can be written in continuous form as:

$$\dot{m}f_{in-cylinder} = (1-\chi)\dot{m}f_{injected} + \frac{mf_{film}}{\tau} \tag{7.2}$$

[a] The film mass alone does not determine the transient response of the fuel delivery.

Where τ is the time constant for the release of fuel film to the combustion chamber and χ is the fraction of injected fuel which is retained in the film. Both τ and χ are different in for different CMCV settings thus an equivalent transient response can result despite different film masses.

Figure 6.3 shows the in-cylinder fuel mass during a rich step in fueling. For both CMCV settings roughly 25 cycles were needed before the delivered in-cylinder fuel mass was equivalent to the injected fuel mass. During these first 25 cycles the fuel film was still being built up. Initially the delivered in-cylinder fuel mass is less than the injected fuel mass. However as the fuel film builds up, the mass of delivered fuel increases; after approximately 25 cycles the active film mass reaches a steady state value and the mass of the delivered fuel is equivalent to the mass of injected fuel.

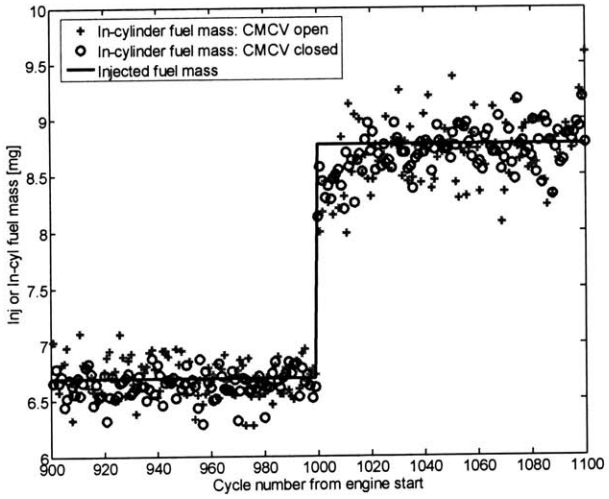

Figure 6.3: Fuel delivery - Rich step in fueling (λ = 1.01 to λ = 0.8)

Figure 6.4 shows the in-cylinder fuel mass during a lean step in fueling. For both CMCV open and closed approximately 40 cycles are needed for the in-cylinder fuel mass to decay to the injected fuel mass. During this decay, the port fuel film mass is shrinking due to the reduced quantity of injected fuel. Initially the mass of fuel which enters the film is less than the mass of fuel leaving the film, however after about 40 cycles the active film mass reaches a steady state value and the delivered fuel mass equals the injected fuel mass.

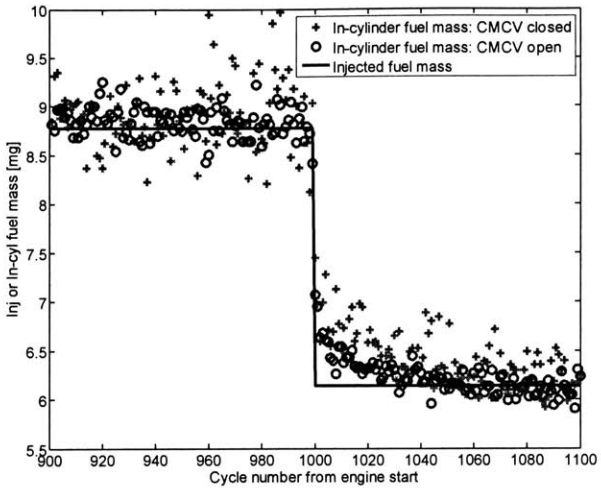

Figure 6.4: Fuel delivery - Lean step in fueling (λ = 0.8 to λ = 1.08)

It is interesting to note that this decay occurs over roughly 40 cycles. This corresponds with the results found earlier, in which the purging mass was equivalent for the first 20 purge cycles for both 250 and 1000 injections. Again during these first 20 purge cycles, fuel was pulled from the downstream and valve films (the active films) which after 250 injections have essentially reached their steady state value. After 20 purge cycles the effect of the differing upstream films begins to take effect. In the transient decay seen in Figure 6.4 it is thought that the initial rich cycles result from films in downstream and valve locations. However as these films are reduced in mass (and thickness) fuel from the upstream films is pulled into downstream locations and subsequently enters the engine. The upstream films have an affect on the fuel delivery although its timescale is different than the downstream and valve films.

Another interesting observation from Figures 6.3 and 6.4 is the increased scatter associated with the CMCV open measurements. This is thought to be the result of the lower intake charge turbulence. This reduced turbulence leads to more variation in the measured in-cylinder pre-flame hydrocarbon concentration. Higher turbulence provides better mixing and thus less scatter.

7 Conclusions

7.1 Experimental

A purging process was used to examine the effect of a CMCV on the port fuel film mass. It was found that the CMCV can provide substantial reductions in the port fuel film mass. These reductions are attributed to the high directed port flow velocity which results from the charge motion plate. This increased velocity improves the in-cylinder fuel transport by providing increased strip atomization of the fuel film.

The effect of different film locations was seen. The downstream (from the injector) and valve films have the most immediate effect on the fuel delivery. Large upstream films can form in areas of reduced air-flow (such as the injector recess) and often provide little influence on the fuel delivery process. These upstream films can take thousands of cycles to slowly develop. The fuel delivery can reach steady state far earlier than the total film mass as the percentage of each injection that contributes to the build-up of upstream films is very small.

The charge motion plate was found to provide substantial reductions in both the total film mass (which includes the less active upstream films) and the initial purge mass. The initial purge mass provides representation of the more active downstream films. After 30 purge cycles, the CMCV has reduced the cumulative purged film mass by approximately 40% indicating that the CMCV provides a substantial reduction in the downstream and valve film mass.

In-cylinder hydrocarbon measurements were made and similar transient responses were observed for both the CMCV open and closed. This similarity despite different film masses was attributed to different τ and χ values. Substantial scatter in these measurements prevented precise calculations of χ.

7.2 Future work

Measurement of the film thickness at various regions in the intake port would provide increased insight on the affect of the CMCV on film formation at different port/manifold locations. This would explicitly demonstrate the ability of the CMCV to reduce the downstream films.

7.3 Recommendations

As HC emission regulations become increasing tight, a reduction in cold-start HC emissions becomes a top priority for future engine designs. It has been shown that a CMCV can provide substantial reductions in the port film mass. This can lead to large reductions in the amount of liquid fuel which enters the chamber during the cold-start process thus reducing cold-start hydrocarbon emissions. The CMCV also provides the benefits of improved combustion stability and thus reduced engine NVH. However the CMCV adds cost and increased complexity to the engine. Furthermore a CMCV complicates engine calibration as the opening of the plate can lead to the rapid release of liquid fuel films. Thus the benefits of a CMCV need to be closely weighed with the increased cost and complexity before implementing such a device.

References

[1] Hirth, P., Holy, G., Bruck, R., "Improved catalyst systems for SULEV legislation: First practical experience" SAE paper 2000-01-0500, 2000.

[2] Park S., et al. "Flow analysis and catalytic characteristics for the various catalyst cell shapes" SAE paper 1999-01-1541, 1999.

[3] Schenck, A., et al., "Engine-Independent Exhaust Gas After-treatment Using a Burner-Heated Catalyst", SAE paper 2006-01-3401, 2006.

[4] Kocks M.W., "Innovative secondary air injection systems" SAE paper 2001-01-0658, 2001.

[5] Shin, Y., Min, K., Cheng, W.K., "Visualization of mixture preparation in a port-fuel injection engine during engine warm-up" SAE paper 952481, 1995.

[6] Shayler, P.J., Winborn, L.D., Scarisbrick A., "Fuel transport to the crankcase, oil dilution and HC return with breather flow during the cold operation of a SI engine" SAE paper 2000-01-1235, 2000.

[7] Stanglmaier, R.H., Li, J., Mathews, R.D., "The effect of in-cylinder, wall-wetting location on the HC emissions from SI engines" SAE paper 1999-01-0502, 1999.

[8] Kim, H., et al., "Correlating port fuel injection to wetted fuel footprints on combustion chamber walls and UBHC in engine start processes" SAE paper 2003-01-3240, 2003.

[9] Curtis, E.W., et al. "A new port and cylinder wall wetting model to predict transient air/fuel excursions in a port fuel injected engine" SAE paper 961186, 1996.

[10] Witze, P.O., Green, R.M., "LIF and flame-emission imaging of liquid fuel films and pool fires in an SI engine during a simulated cold start" SAE paper 970866, 1997.

[11] Shin, Y., Cheng, W.K., Heywood, J.B., "Liquid gasoline behavior in the engine cylinder of a si engine" SAE paper 941872, 1994.

[12] Meyer, R., Heywood, J.B., "Liquid fuel transport mechanisms into the cylinder of a firing port-injected SI engine during start up" SAE paper 970865, 1997.

[13] Skippon, S.M., Norton, D., "The effects of gasoline volatility on mass and composition of the inlet port wall film in port-injected SI engines" SAE paper 982517, 1998.

[14] Landsberg, G.B., Heywood, J.B., Cheng, W.K., "Contribution of liquid fuel to hydrocarbon emissions in spark ignition engines" SAE paper 2001-01-3587, 2001.
[15] Meyer, R., Yilmaz, E., Heywood, J.B., "Liquid fuel flow in the vicinity of the intake valve of a port-injected SI engine", SAE paper 982471, 1998.
[16] Hentschel W., Grote, A., Langer, O., "Measurement of wall film thickness in the intake manifold of a standard production SI engine by a spectroscopic technique", SAE paper 972832, 1997.
[17] Cheng, C., et al., "Intake port phenomena in a spark-ignition engine at part load", SAE paper 912401, 1991.
[18] Aquino, C.F., "Transient A/F control characteristics of the 5 liter central fuel injection engine", SAE paper 810494, 1981.
[19] Lee, D., "Effects of Charge Motion Control During Cold Start of SI Engines", Masters Thesis, Mechanical Engineering, MIT, 2005.
[20] Kim, H., et al., "Effects of Injection Timings and Intake Port Flow Control on the In-Cylinder Wetted Fuel Footprints During PFI Engine Startup Process" SAE paper 2005-01-2082, 2005.
[21] Crouse, W.H., Anglin D.L., "Automotive Mechanic Book", New York: McGraw-Hill, 2002.
[22] ASTM D86-05 Standard Test Method for Distillation of Petroleum Products at Atmospheric Pressure
[23] ASTM D323-06 Standard Test Method for Vapor Pressure of Petroleum Products (Reid Method)
[24] Chevron Phillips UTG-91 fuel specifications
[25] Kenney, T., et al "Acquisition and Analysis of Cylinder Pressure Data Recommended Procedures", GM internal paper, 1992.
[26] Cambustion HFR400 Fast FID Manual, Version 3.2, 2000.
[27] Cambustion website, http://cambustion.com
[28] Heywood, J.B., "Internal Combustion Engine Fundamentals", New York: McGraw-Hill, 1988.
[29] Cheung, H.M., "A practical burn rate analysis for use in engine development and design." Masters Thesis, Mechanical Engineering, MIT, 1993.

[30] Conversation with Erik Curtis

[31] Lee, S., et al., "Effects of swirl and tumble on mixture preparation during cold start f a gasoline direct-injection engine", SAE paper 2000-01-1900, 2000.

[32] Meyer, R., Heywood, J.B., "Evaporation of in-cylinder liquid fuel droplets in an SI engine: A diagnostic-based modeling study", SAE paper 1999-01-0567, 1999.

[33] Giansetti, P., et al., "Residual Gas Fraction Measurement in Spark Ignition Engines", SAE paper 2005-24-078, 2005.

[34] Cho, H., et al., "Measurements and modeling of residual gas fraction in SI engines", SAE paper 2001-01-1910, 2001.

[35] Galliot, F., et al., "In-cylinder measurements of residual gas concentration in a spark ignition engine", SAE paper 900485, 1990.

(this page was left intentionally blank)

Appendix A: Fuel mass contained in each purge cycle

The total number of moles contained in the in-cylinder charge is given by:

$$n_{tot} = n_{HC1} + n_{air} \tag{A.1}$$

This can be rewritten:

$$n_{tot} = n_{HC1}\left(1 + \frac{n_{air}}{n_{HC1l}}\right) \tag{A.2}$$

From the definition of molecular weight:

$$n_i = {}^{m_i}\!/_{MW_i} \tag{A.3}$$

Substituting equation (3) into equation (2):

$$n_{tot} = n_{HC1}\left\{1 + \left(\frac{MW_{HC1}}{MW_{air}}\right)\left(\frac{m_{air}}{m_{HC1}}\right)\right\} \tag{A.4}$$

The concentration of HC1 in the fresh charge is given by:

$$x_{HC1} = \left(\frac{n_{HC1}}{n_{tot}}\right) = \frac{1}{1 + \left(\frac{m_{air}}{m_{HC1}}\right)\left(\frac{MW_{HC1}}{MW_{air}}\right)} \tag{A.5}$$

Solving for $m_{HC1} = m_{fuel\ per\ cycle}$

$$m_{fuel\ per\ cycle} = m_{air\ per\ cycle}\left(\frac{x_{HC1}}{1 - x_{HC1}}\right)\left(\frac{MW_{HC1}}{MW_{air}}\right) \tag{A.6}$$

Appendix B: Determination of the pre-flame hydrocarbon concentration

The total number of moles contained in the in-cylinder charge is given by:

$$n_{tot} = n_{fuel} + n_{air} + n_{res} \tag{B.1}$$

This can be rewritten:

$$n_{tot} = n_{fuel}\left(1 + \frac{n_{air}}{n_{fuel}}\right) + n_{res} \tag{B.2}$$

The following simple relations can be used to further reduce equation (2):

$$n_i = {}^{m_i}\!/_{MW_i} \tag{B.3}$$

$$n_{res} = x_{res} n_{tot} \tag{B.4}$$

Substituting equations (3) and (4) into equation (2):

$$n_{tot} = n_{fuel}\left\{1 + \left(\frac{MW_{fuel}}{MW_{air}}\right)\left(\frac{m_{air}}{m_{fuel}}\right)_{in-cyl}\right\} + x_{res} n_{tot} \tag{B.5}$$

Solving equation (5) for n_{tot}:

$$n_{tot} = \frac{n_{fuel}\left\{1 + \left(\frac{MW_{fuel}}{MW_{air}}\right)\left(\frac{m_{air}}{m_{fuel}}\right)_{in-cyl}\right\}}{1 - x_{res}} \tag{B.6}$$

The concentration of HC1 in the fresh charge is given by:

$$x_{HC1} = x_{fuel}\left(\frac{MW_{fuel}}{MW_{HC1}}\right) = \left(\frac{n_{fuel}}{n_{tot}}\right)\left(\frac{MW_{fuel}}{MW_{HC1}}\right) \tag{B.7}$$

Substituting equation (6) for n_{tot} into equation (7), the HC1 concentration is given by:

$$x_{HC1} = \left(\frac{MW_{fuel}}{MW_{HC1}}\right)\frac{1 - x_{res}}{\left\{1 + \left(\frac{MW_{fuel}}{MW_{air}}\right)\left(\frac{m_{air}}{m_{fuel}}\right)_{in-cyl}\right\}} \tag{B.8}$$

Finally equation (8) can be solved for the in-cylinder air-fuel ratio:

$$\left(\frac{m_{air}}{m_{fuel}}\right)_{in-cyl} = \left\{\left(\frac{1 - x_{res}}{x_{HC1}}\right)\left(\frac{MW_{fuel}}{MW_{HC1}}\right) - 1\right\}\frac{MW_{air}}{MW_{fuel}} \tag{B.9}$$

Appendix C: τ-χ model

The τ-χ model first developed by [18] is a widely used open-loop fuel film compensation algorithm that is used the fueling control system. The τ-χ model in continuous form can be written as:

$$\dot{m}f_{purge} = \frac{mf_{film}}{\tau} \qquad \text{(C.1)}$$

τ is the time constant for the release of fuel film to the combustion chamber
χ is the fraction of injected fuel which is retained in the film.

The discrete form of the τ-χ model can be obtained by integrating equation C.1 over one cycle:

$$mf_{in-cylinder,i} = (1-\chi)mf_{injected,i} + \frac{mf_{film,i}}{\tau/\Delta t} \qquad \text{(C.2)}$$

At steady state the film mass reduces to:

$$mf_{film,SS} = \chi\left(\tau/\Delta t\right)mf_{injected,SS} \qquad \text{(C.3)}$$